Inhibition of Karyopherin β1-mediated nuclear import disrupts oncogenic lineage-defining transcription factor activity in small cell lung cancer

Demetra P. Kelenis[1], Rahul K. Kollipara[2], Karine Pozo[1,3], Kathia E. Rodarte[1], Shreoshi Pal Choudhuri[3], Kyle B. Spainhower[4], Sarah J. Wait[4], Victor Stastny[5], Trudy G. Oliver[4], and Jane E. Johnson[1,*].

[1]Department of Neuroscience, [2]McDermott Center for Human Growth and Development, [3]Department of Internal Medicine, UT Southwestern Medical Center, Dallas, TX 75390, USA, [4]Department of Oncological Sciences, Huntsman Cancer Institute, University of Utah, Salt Lake City, UT 84112, USA, [5]Hamon Center for Therapeutic Oncology Research, UT Southwestern Medical Center, Dallas, TX 75390, USA.

*Lead Contact and Correspondence: jane.johnson@utsouthwestern.edu

Conflict of Interest Disclosure:

The authors declare no potential conflicts of interest.

ABSTRACT

Genomic studies support the classification of small cell lung cancer (SCLC) into subtypes based on expression of lineage-defining transcription factors ASCL1 and NEUROD1, which together are expressed in ~86% of SCLC. ASCL1 and NEUROD1 activate SCLC oncogene expression, drive distinct transcriptional programs, and maintain the *in vitro* growth and oncogenic properties of ASCL1 or NEUROD1-expressing SCLC. ASCL1 is also required for tumor formation in SCLC mouse models. A strategy to inhibit the activity of these oncogenic drivers may therefore provide both a targeted therapy for the predominant SCLC subtypes, and a tool to investigate the underlying lineage-plasticity of established SCLC tumors. However, there are no known agents that inhibit ASCL1 or NEUROD1 function. In this study, we identify a novel strategy to pharmacologically target ASCL1 and NEUROD1 activity in SCLC, by exploiting the nuclear localization required for these transcription factors' function. We identify Karyopherin β1 (KPNB1) as a nuclear import receptor for ASCL1 and NEUROD1 in SCLC, and demonstrate that the inhibition of KPNB1 leads to impaired ASCL1 and NEUROD1 nuclear accumulation and transcriptional activity. Pharmacologic targeting of KPNB1 preferentially disrupts the growth of ASCL1/NEUROD1+ SCLC *in vitro,* and ASCL1+ tumor growth *in vivo*, an effect mediated by a combination of impaired ASCL1 downstream target expression, cell cycle activity, and proteostasis. These findings broaden the support for targeting nuclear transport as an anticancer therapeutic, and have implications for targeting lineage transcription factors in tumors beyond SCLC.

SIGNIFICANCE

This work identifies Karyopherin β1 (KPNB1) as a nuclear import receptor for lineage-defining transcription factors ASCL1 and NEUROD1 in SCLC, and suggests that pharmacologic targeting of KPNB1 indirectly inhibits the activity of these oncogenic drivers in SCLC.

INTRODUCTION

Small cell lung cancer (SCLC) is an aggressive neuroendocrine tumor. SCLC is one of the most lethal human malignancies, and is one of two cancers designated as “recalcitrant” by the NCI and US Congress due to its rapid development of resistance to conventional chemotherapy (1-3). Despite genomic studies revealing widespread inactivation of tumor suppressors TP53 and RB1, and high MYC family expression, there are currently no molecularly targeted therapies for this disease (2,4,5). Recent large-scale genomic studies of human and mouse SCLC models support the classification of SCLC into distinct subtypes based on the expression or absence of lineage-defining transcription factors: ASCL1 (SCLC-A), NEUROD1 (SCLC-N), and POU2F3 (SCLC-P). Together, SCLC-A and SCLC-N comprise a majority of SCLC, with 86% of tumors expressing ASCL1 and/or NEUROD1 (6,7).

ASCL1 and NEUROD1 are basic helix-loop-helix (bHLH) transcription factors (TFs) essential for neuronal differentiation during embryonic development (8-11). ASCL1 is also required for the differentiation of pulmonary neuroendocrine cells (PNECs), rare neuroendocrine cells that serve as cells of origin for SCLC (12,13). Deletion of TP53 and RB1 in adult PNECs gives rise to ASCL1+ tumors in multiple genetically engineered mouse models (GEMMs) of SCLC (14-16), where ASCL1 has been shown to be essential for tumor formation, and shown to drive expression of neuroendocrine (NE) lineage genes such as INSM1, NCAM1 and CHGA (17). Both ASCL1 and NEUROD1 are known to command the expression of multiple oncogenes underlying SCLC progression, such as RET and MYC, respectively (17). Both TFs also play key roles in maintaining the *in vitro* growth, proliferation, and migration of SCLC-A and SCLC-N cell lines (17-22), and confer distinct molecular and physiological properties to these subtype specific tumor models (6,17). Thus, strategies to inhibit ASCL1 and NEUROD1 activity may provide both an attractive, targeted SCLC therapy, and a tool to investigate the consequences of lineage-transcription factor loss in SCLC tumors that have already formed. Unfortunately,

there are no known agents that inhibit the function of ASCL1 or NEUROD1, consistent with long-standing difficulties in targeting TFs.

ASCL1 and NEUROD1 activate expression of their downstream target genes by heterodimerizing with an E-protein bHLH factor and binding to DNA at E-box consensus sequences, where transcriptional activation occurs following the recruitment of co-activators (23-26). Therefore, in order to bind to DNA and activate transcription, ASCL1 and NEUROD1 must first travel from their sites of translation in the cytoplasm into the nucleus. In eukaryotes, the nucleocytoplasmic exchange of proteins and other molecules occurs through the highly selective nuclear pore complexes embedded within the nuclear envelope (27,28). In humans, the cytoplasmic to nuclear transport of molecules too large to passively diffuse through the nuclear pore complex at physiologically relevant timescales (29) is mediated by the Karyopherin β superfamily of nuclear transport receptors. This nuclear transport mechanism is RanGTP-dependent, and the specificity of a given transport receptor for a particular cargo protein is conferred by the presence of a nuclear localization signal (NLS) within the cargo (27).

Interestingly, it has been shown in neuronal cell culture models that NEUROD1 is selectively imported into the nucleus by a member of the Karyopherin β superfamily known as Karyopherin β1 (also known as Importin β1 or KPNB1). Here, the interaction of NEUROD1 with its E-protein binding partner TCF3 exerts a synergistic effect that promotes the KPNB1-mediated nuclear import of NEUROD1/TCF3 heterodimers over the import of monomeric NEUROD1 alone (30,31). Additionally, the muscle-specific bHLH TF MYOD, which shares the same E-protein binding partners with both NEUROD1 and ASCL1, is also imported into the nucleus via KPNB1, suggesting a conserved nuclear import mechanism for this family of TFs (30,31). Nonetheless, whether ASCL1 is also imported into the nucleus by KPNB1, and whether NEUROD1 is imported into the nucleus by KPNB1 in the context of SCLC, had not been studied.

KPNB1 is highly expressed in multiple cancers (32) where it is implicated in the nuclear translocation of EMT-promoting proteins SMAD, SNAIL, and NOTCH (33-35), inflammation-associated TFs NFκB and AP-1 (36), and immune checkpoint protein PD-L1 (37). KPNB1 also plays a key role in regulating multiple aspects of mitosis, including mitotic spindle formation, and nuclear membrane and pore assembly (38,39). KPNB1 is targetable with several potent, cell permeable inhibitors that have been pursued as an anti-tumor strategy in lung adenocarcinoma, cervical, breast, ovarian, gastric and prostate cancer models, among others (27,32,40,41). In these models, KPNB1 inhibition disrupted PDX growth or triggered cell cycle arrest and apoptosis, without disrupting the growth of noncancer cells at the same concentrations (40,42,43). However, KPNB1 inhibition in SCLC has not been reported, where KPNB1 inhibitors may have the added ability to deprive SCLC cells of ASCL1 and NEUROD1 activity by blocking the access of the TFs to the nucleus, thereby disrupting the growth of SCLC subtypes with a known dependence on ASCL1 or NEUROD1 (17-22).

Here, we implicate KPNB1 as a significant nuclear import receptor for the lineage-defining TFs ASCL1 and NEUROD1 in SCLC, and investigate the inhibition of KPNB1-mediated nuclear import as a strategy to disrupt ASCL1 and NEUROD1 function in this disease.

RESULTS

KPNB1 is expressed across SCLC models

Comparison of RNA-sequencing data from multiple SCLC models, including 81 patient primary tumor samples (5), 32 SCLC PDXs (44), and 70 human SCLC cell lines (45), revealed that *KPNB1* is broadly expressed across SCLC subtypes (Figure 1A-B). Following clustering of the primary tumors into ASCL1-expressing SCLC-A, NEUROD1-expressing SCLC-N, POU2F3-expressing SCLC-P, and YAP1-expressing SCLC-Y subtypes using described gene signatures (6,17), *KPNB1* expression was found to be significantly higher in the SCLC-A tumors in comparison to the SCLC-P and SCLC-Y tumors (Figure 1A), though all subtypes expressed

high levels of *KPNB1*. In human cell lines, though *KPNB1* expression is slightly higher in SCLC-N than in SCLC-A (Figure 1B), KPNB1 is highly expressed across all SCLC subtypes, NSCLC cell lines with neuroendocrine features (NSCLC-NE), and immortalized human bronchial epithelial cells (HBEC) (Figure 1B,C).

KPNB1 interacts with ASCL1 and NEUROD1 in SCLC-A and SCLC-N cells

To activate transcription, ASCL1 and NEUROD1 must travel from their sites of translation in the cytoplasm back into the nucleus, a process that for most proteins occurs through binding with members of the Karyopherin-β family of nuclear transport receptors (32), including KPNB1. Given the ubiquitous KPNB1 expression in SCLC, we investigated whether KPNB1 interacts with ASCL1 or NEUROD1. We previously identified candidate ASCL1 binding partners by mass spectrometry analysis of proteins immunopurified with ASCL1 from SCLC-A subtype NCI-H2107 cells (46) (Figure 1D). Through this analysis, KPNB1 was identified as an ASCL1 interactor (Figure 1E). Though no other nuclear import receptors were identified as candidate ASCL1 binding partners, KPNA2 (Karyopherin subunit alpha 2), a Karyopherin alpha adaptor protein that interacts with both KPNB1 and its' cargo via the NLS (32), was also identified as an ASCL1 interactor, strengthening the potential role of KPNB1 in the nuclear import of ASCL1. For comparison, the known ASCL1 E-protein binding partners TCF3, TCF4, and TCF12 were also identified (Figure 1E) (see (46) for complete list of identified proteins). Validating the mass spectrometry-identified ASCL1/KPNB1 interaction, KPNB1 and ASCL1 co-immunoprecipitated from the SCLC-A cell line models NCI-H2107 and NCI-H889 (Figure 1F). Additionally, the interaction between NEUROD1 and KPNB1 in SCLC-N was demonstrated by co-immunoprecipitation from the SCLC-N cell lines NCI-H524 and NCI-H2171 (Figure 1G).

KPNB1 knockdown reduces nuclear ASCL1 in SCLC-A

The interaction between ASCL1 and nuclear transport receptor KPNB1 in SCLC-A cells suggests that KPNB1 may mediate the nuclear import of this lineage oncogene in SCLC. To test this, we knocked down KPNB1 in the SCLC-A cell line NCI-H2107, followed by subcellular

fractionation and western blotting to compare the levels of ASCL1 in the nuclear, cytoplasmic, and whole cell lysate fractions of cells transfected with KPNB1 siRNA (siKPNB1) versus control siRNA (siCtrl) at 24 and 48 hours post-transfection. With a 70% knockdown of KPNB1 protein (Figure 2A), we observed a 50% reduction in the amount of ASCL1 protein in the nuclear fraction at 48 hours post-transfection (Figure 2B red square, D quantification). KPNB1 knockdown also led to a reduction in whole cell ASCL1 (Figure 2C) with no increase in the cytoplasmic fraction, suggesting that accumulating cytoplasmic ASCL1 may be rapidly degraded as described in ASCL1-expressing neural stem cells (47,48).

KPNB1 knockdown reduces expression of ASCL1 downstream target genes

To bind E-box containing DNA and activate transcription of downstream target genes, ASCL1 and its E-protein binding partner must be localized to the nucleus. Given the reduction in nuclear ASCL1 protein observed following KPNB1 knockdown, we next tested the effect of KPNB1 knockdown on the expression of known ASCL1 downstream target genes, including NOTCH ligand genes (23,49,50), SCLC oncogenes, and NE markers (17) in NCI-H2107 cells (Figure 2E). KPNB1 knockdown resulted in significantly decreased expression of the NOTCH ligand gene *DLL1*, SCLC oncogenes *MYCL*, *BCL2*, *NFIB*, *RET* and *SOX2*, NE markers *INSM1* and *NCAM1*, and lung-lineage gene *FOXA2* (Figure 2E, red bars). Consistently, ASCL1 knockdown in the same cell line (Figure 2E, green bars) resulted in reduced expression of the same panel of ASCL1 targets. Together, these findings suggest that in SCLC-A, ASCL1 is imported into the nucleus in a KPNB1-mediated manner, and that KPNB1-dependent mechanisms play a role in expression of genes previously shown to promote SCLC growth, NE, and lung cell identity.

To control for potential off-target effects of the KPNB1 siRNAs, we also tested whether an exogenous, siRNA-resistant form of KPNB1 could rescue nuclear ASCL1 protein levels and ASCL1 downstream target expression following KPNB1 knockdown. We generated a doxycycline (Dox)-inducible lentiviral construct expressing an siRNA-resistant form of KPNB1

(Supplemental Figure S1A, “ResKPNB1”), where silent mutations were introduced in the *KPNB1* coding sequence to prevent targeting by the KPNB1 siRNAs used (Supplemental Table S1). Expression of this KPNB1 construct fully rescued nuclear ASCL1 protein levels (Supplemental Figure S1D), expression of a majority of the ASCL1 downstream targets genes assessed (Supplemental Figure S1E), and the growth of the cells following siKPNB1 transfection (Supplemental Figure S1F), suggesting that these phenotypes were specific to the KPNB1 knockdown.

To confirm the phenotype seen with KPNB1 siRNA knockdown, we also used CRISPR interference-mediated repression (CRISPRi) (51,52) to repress KPNB1 expression in SCLC-A. The lentiviral construct shown in Figure 2F (53) was used to generate SCLC-A subtype NCI-H2107 cell lines expressing catalytically inactive Cas9 (dCas9) fused to the KRAB transcriptional repressor in addition to one of two gRNAs directed against the 5’ UTR of *KPNB1* (Figure 2F, gKPNB1.1 and gKPNB1.2). Using this CRISPRi KPNB1 system, we obtained an 84% reduction in KPNB1 protein (Figure 2G) at 1 week post-transduction and selection with puromycin. In the CRISPRi KPNB1 cells, nuclear ASCL1 protein was reduced 50% relative to control (Figure 2H, I). Taken together, our observations following both CRISPRi and siRNA-mediated repression of KPNB1, suggest that ASCL1 nuclear levels depend on KPNB1 in the setting of SCLC, and that the inhibition of KPNB1 may provide a way to disrupt ASCL1 transcriptional activity.

Repression of KPNB1 leads to repression of the ASCL1 transcriptional program

KPNB1 mediates the nuclear import of numerous cargos aside from ASCL1. To investigate the extent to which KPNB1 depletion disrupts the transcriptional activity of ASCL1, we next compared changes in the transcriptome following direct repression of ASCL1 versus KPNB1 in SCLC-A subtype NCI-H2107 cells using RNA-seq. The lentiviral dCas9-KRAB system (Figure 2F) with gRNAs ASCL1.1 and ASCL1.2 targeting near the *ASCL1* transcription start site, resulted in undetectable ASCL1 protein by western blot (Figure 2J). RNA-seq was performed at

1 week post-transduction and puromycin selection (n=2 Empty Vector or CRISPRi ASCL1). 355 differentially expressed genes (DEG) were identified between controls and CRISPRi ASCL1 cells, including significantly reduced expression of previously identified ASCL1 downstream targets (17) *DLL3*, *INSM1*, and *RET* (Supplemental Table S2). Likewise, RNA-seq from the CRISPRi KPNB1 cell lines at 1 week post-transduction (n=2 CRISPRi KPNB1), identified 6,510 DEG (Supplemental Table S2). To examine the effect of KPNB1 depletion on ASCL1 transcriptional activity, we compared expression of the 355 DEG identified following direct CRISPRi-mediated repression of ASCL1 between the CRISPRi KPNB1 cell lines, CRISPRi ASCL1 cell lines, and siASCL1 knockdown NCI-H2107 cells previously profiled by RNA-seq (46), where the heatmap shown in Figure 2K displays fold change of these 355 DEG relative to the respective empty vector controls. While not perfectly aligned, the DEG in the CRISPRi KPNB1 cells reflect the pattern seen with the direct repression of ASCL1 expression (Figure 2K). This is also demonstrated with gene set enrichment analysis (GSEA) where the CRISPRi KPNB1 cells were significantly depleted for the subset of DEG downregulated following direct CRISPRi-mediated repression of ASCL1 (Figure 2L), and significantly enriched for the DEG upregulated upon CRISPRi ASCL1 (Figure 2M). Taken together, our findings support the conclusion that KPNB1 inhibition disrupts the transcriptional activity of ASCL1 in SCLC-A. Nonetheless, the expression of some ASCL1 DEG were differentially affected by direct repression of ASCL1 versus KPNB1 in the NCI-H2107 cells (Figure 2K). Thus, although KPNB1 depletion results in gene expression changes consistent with direct repression of ASCL1 expression, not all ASCL1 targets genome-wide support this relationship, likely reflecting the activity of other proteins dependent on KPNB1 nuclear transport.

KPNB1 depletion reduces nuclear NEUROD1, and NEUROD1 downstream target expression in SCLC-N

Given our evidence of a NEUROD1/KPNB1 interaction in SCLC-N cells (Figure 1G), we also examined the effect of KPNB1 siRNA knockdown on the levels of nuclear NEUROD1 in the

SCLC-N cell line NCI-H2171. Here, a 60% knockdown of KPNB1 protein (Figure 3A) led to a 50% reduction in nuclear NEUROD1 at 48 and 72 hours post-siRNA transfection (Figure 3A red box, B quantification). To control for siRNA off-target effects, we also tested the ability of the siRNA-resistant KPNB1 construct (ResKPNB1) (Supplemental Figure S2A) to rescue nuclear NEUROD1 protein levels following KPNB1 knockdown, where ResKPNB1 expression partially rescued nuclear NEUROD1 (Supplemental Figure S2D). Given the impaired nuclear accumulation of NEUROD1 in the KPNB1 knockdown cells, we examined the effect of KPNB1 knockdown on the expression of previously identified NEUROD1 downstream target genes (Figure 3C) (17) including the SCLC oncogene *MYC*, which has been shown to be amplified in SCLC-N tumors and cell lines, and the NE markers *NCAM1* and *INSM1*. Here, we observed significantly decreased expression of *MYC* and *NCAM1*, but not *INSM1* (Figure 3C). These findings suggest that KPNB1-mediated nuclear import of NEUROD1 may play a role in regulating the expression of genes important for SCLC-N growth and NE identity, though this effect was less dramatic than that seen for ASCL1 in SCLC-A.

We also repressed KPNB1 expression in NCI-H2171 cells using the dCas9-KRAB system shown in Figure 2F, obtaining a 50-70% reduction in KPNB1 protein (Figure 3D), and 40-50% reduction in nuclear NEUROD1 (Figure 3E, F), consistent with the KPNB1 siRNA knockdown. Together, the impaired nuclear import of NEUROD1 seen following both siRNA knockdown and CRISPRi-mediated repression of KPNB1 suggests that NEUROD1 is imported into the nucleus by KPNB1 in SCLC-N, extending prior findings in neuronal cell lines (30,31) to SCLC.

Pharmacologic inhibition of KPNB1 impairs the nuclear accumulation of ASCL1 and NEUROD1 in SCLC

Given the reduced nuclear ASCL1 and NEUROD1 observed following genetic depletion of KPNB1, we next examined the effect of KPNB1 pharmacologic inhibition on the nuclear accumulation of ASCL1 and NEUROD1 in SCLC cell lines. We tested two KPNB1 inhibitors with

differing mechanisms of action: Importazole (IPZ) (54), and Inhibitor of Nuclear Import-43 (INI-43) (40). SCLC-A subtype NCI-H2107, and SCLC-N subtype NCI-H2171 cells were treated with their respective IC50 concentrations of IPZ or INI-43 (Supplemental Figure S3) followed by comparison of the levels of ASCL1 and NEUROD1 in the nuclear protein fractions at 24 hours post-treatment. Treatment of NCI-H2107 cells with IPZ or INI-43 resulted in a 61% or 36% decrease, respectively, in nuclear ASCL1 relative to vehicle-treated cells (Figure 4A, C). Treatment of NCI-H2171 cells with IPZ or INI-43 resulted in a 70% or 50% decrease, respectively, in nuclear NEUROD1 (Figure 4B, D). For all conditions, cytoplasmic ASCL1 or NEUROD1 was low and not significantly altered by KPNB1 inhibitor treatment (data not shown), consistent with our observations following KPNB1 genetic depletion in the same cell lines. Together, pharmacologic, siRNA, and CRISPRi strategies to inhibit KPNB1 all led to reduced nuclear accumulation of ASCL1 or NEUROD1 in SCLC-A or -N cells, respectively, supporting KPNB1's role in mediating the nuclear import of these transcription factors in SCLC.

Pharmacologic inhibition of KPNB1 preferentially disrupts the growth of SCLC-A and -N subtypes over SCLC-P

KPNB1 is a key regulator of mitosis (38) and is required for the proliferation of multiple cancer cell lines, where KPNB1 inhibition triggers G2/M cell cycle arrest and apoptosis without affecting the growth of noncancer cells at the same doses (32,40,43). However, KPNB1 inhibition in SCLC had not been previously reported. We tested the effects of the KPNB1 inhibitor INI-43 on SCLC-A, SCLC-N, and SCLC-P cell lines in cell viability, cell cycle, and colony formation in soft agar assays (Figure 5). In both cell viability and soft agar assays, SCLC-A and SCLC-N cell lines were more sensitive to INI-43 treatment than SCLC-P cell lines (Figure 5A-D), despite similar KPNB1 expression levels (Figure 1B, C). Given that SCLC-P cells do not express ASCL1 or NEUROD1, the preferential toxicity of INI-43 in the SCLC-A and -N cell lines is consistent with impaired nuclear import of lineage oncogenes ASCL1 and NEUROD1 contributing to the growth disruption observed following KPNB1 inhibition, though differences in

INI-43 uptake or metabolism between the different subtypes cannot be excluded. Consistent with prior reports (32,40,43), short term treatment with a high-dose of INI-43 led to an increased percentage of cells in the G2/M phase of the cell cycle, and a reduced percentage of cells in G0/G1, in cell lines representing all three SCLC subtypes (Figure 5E). These results suggest that the preferential toxicity of INI-43 in SCLC-A and SCLC-N may be mediated by effects aside from the mitotic block caused by this drug.

KPNB1-independent nuclear accumulation of ASCL1 rescues SCLC-A growth following KPNB1 inhibition

Given that ASCL1 or NEUROD1 are known to maintain the *in vitro* growth and oncogenic properties of ASCL1 or NEUROD1-expressing SCLC cell lines (17-22), the preferential disruption of SCLC-A and -N growth observed following KPNB1 inhibition may result from reduced nuclear import of ASCL1 or NEUROD1, or may just reflect previously reported broad effects of KPNB1 inhibition in cancer cells (32). To distinguish between the contribution of each mechanism, we designed Dox-inducible expression constructs for ASCL1 and NEUROD1 that would localize to the nucleus independent of KPNB1 activity (Figure 6A, B). A proline-tyrosine nuclear localization signal (PY-NLS) from the RNA binding protein hnRNP M was added to the N-termini of ASCL1 and NEUROD1 to confer specificity for a nuclear import receptor other than KPNB1. This PY-NLS has been shown to bind with high affinity to the Transportin-1 (also known as KPNB**2**) nuclear transport receptor (55). To prevent KPNB1 from binding to exogenously expressed ASCL1 and NEUROD1, all basic amino acids within the endogenous NLSs of both proteins (31,56), JEJ unpublished) were mutated to alanine (Figure 6A, ASCL1* or NEUROD1*), given that nonspecific clusters of basic amino acids can bind to nuclear import receptors in the absence of a canonical NLS (57). Wild-type (WT) ASCL1 or NEUROD1 were used as controls. We generated SCLC-A NCI-H2107 or SCLC-N NCI-H2171 cell lines expressing PY-NLS-ASCL1* or PY-NLS-NEUROD1* respectively, versus the corresponding WT-controls. We then tested the effects of 0.5, 1.5, and 3 μM doses of INI-43 on the viability of

these cell lines at 1-4 days post-treatment (Figure 6C, D, Supplemental Figure S4A,B). In the SCLC-A cells, PY-NLS-ASCL1* expression partially rescued growth following treatment with both 0.5 μM and 1.5 μM INI-43 (Supplemental Figure S4A), and led to a significantly increased number of viable cells at 1-4 days post-treatment with both doses of the drug (Figure 6C). These observations suggest that reduced nuclear import of ASCL1 is responsible for a substantial portion of the growth inhibitory effect of INI-43 in this cell line. In contrast, PY-NLS-NEUROD1* expression in the SCLC-N cells did not lead to a significant increase in cell viability following 1.5 μM INI-43 treatment (Figure 6D, Supplemental Figure S4B), despite fully rescuing nuclear NEUROD1 protein at this dose (Supplemental Figure S4E,F). Together, these findings suggest that reduced nuclear translocation of ASCL1 plays a greater role in the growth disruptive effects of KPNB1 inhibition in SCLC-A, than the reduced nuclear translocation of NEUROD1 in SCLC-N, a finding consistent with NEUROD1's more dispensable role in the growth of the SCLC-N subtype (17,18,58).

In vivo pharmacologic inhibition of KPNB1 disrupts SCLC-A patient derived xenograft growth

We next examined the *in vivo* antitumor activity of the KPNB1 inhibitor INI-43 in a SCLC-A patient derived xenograft (PDX) model of SCLC, JHU-LX44, and a SCLC-N PDX model, JHU-LX22. Though both PDX models express nearly identical levels of *KPNB1* RNA, JHU-LX44 tumors have high *ASCL1*, while the JHU-LX22 tumors have high *NEUROD1* and low *ASCL1*, consistent with their SCLC-A or -N classification (Figure 7A). PDX-bearing mice were treated with 25 mg/kg INI-43 every 48 hours for 10-16 days, where INI-43 inhibited the growth of the SCLC-A, but not SCLC-N tumors (Figure 7B vs. C). Pharmacokinetic analysis of INI-43 concentrations revealed significantly higher levels of INI-43 in tumor tissue in comparison to plasma, and stable concentrations from 2 to 24 hours post-treatment (Figure 7D), suggesting active accumulation or retention of INI-43 in the tumors. These findings highlight the potential clinical relevance of KPNB1 inhibition in ASCL1+ SCLC.

KPNB1 inhibition leads to increased translation-associated gene expression and enrichment for proteasomal pathways in both SCLC-A and -N tumors

To uncover gene expression changes due to KPNB1 inhibition, we performed RNA-seq analysis on tumors harvested at the end of the treatment schedules shown Figure 7B and C. Comparing the transcriptomes between vehicle-treated and INI-43-treated PDXs revealed many DEG following treatment with INI-43 (Supplemental Table S3, FDR<0.05). In both SCLC-A and -N tumors, INI-43-treatment led to the upregulation of numerous genes involved in translation, including ribosomal proteins ("RPL" and "RPS"), mitochondrial ribosomal proteins ("MRP"), elongation and initiation factors ("EEF" and "EIF"), as well as histone-encoding genes ("HIST") (Figure 7E-F, Supplemental Table S3). Together, the upregulation of RPS/RPL/MRP genes is suggestive of a global up-regulation of the transcriptome, rRNA synthesis, and translational output (59) which has been shown to impair differentiation and increase apoptosis in neural stem cells (60). In addition, KPNB1 inhibition also disrupted proteostasis as evidenced by the upregulation of numerous proteasomal subunit ("PSM") and ubiquitin-related ("UBA/B/E/L/T") genes (Figure 7F, Supplemental Table S3). This is consistent with a prior report (61) where pharmacologic inhibition of KPNB1 in glioblastoma cells led to increased ubiquitination, proteasome-mediated degradation, and induction of unfolded protein response (UPR)-mediated apoptosis. Together, the increased translation-associated gene expression, and enrichment for proteasomal pathways observed following KPNB1 inhibition in the SCLC-A and -N PDX models suggests that though disrupted proteostasis is one consequence of KPNB1 inhibition, this alone is not sufficient for suppressing SCLC tumor growth since only the SCLC-A PDXs exhibited suppressed growth following KPNB1 targeting.

Decreased cell cycle activity and ASCL1 downstream target expression underlie the anti-tumor activity of KPNB1 inhibition in SCLC-A

We found that *in vivo* pharmacologic inhibition of KPNB1 disrupts SCLC-A, but not SCLC-N PDX growth (Figure 7B, C) suggesting there are additional mechanisms contributing to the

growth inhibitory effect of INI-43 observed in the SCLC-A tumors. The identification of pathways unique to the INI-43-treated SCLC-A tumors may provide insight into these mechanisms. To this end, we next excluded the ribosomal (RPS/RPL/MRPL), elongation/initiation factor (EEF/EIF), proteasomal (PSM), and histone (HIST) genes from the DEG identified in the INI-43-treated SCLC-A and SCLC-N PDXs, given that the involvement of these genes in numerous processes overshadow further pathway analysis (Figure 7G, modified DEG, Supplemental Table S3).

The DEG that were unique to the INI-43-treated SCLC-A PDX samples were depleted for numerous cell-cycle related pathways reflected by Reactome terms “Mitotic prometaphase”, “Resolution of sister chromatid cohesion”, and “Cell cycle”, among others (Figure 7G, Supplemental Table S3) consistent with the reported role of KPNB1 in regulating multiple mitotic events (38). INI-43 treatment in the SCLC-A PDX model also led to significantly reduced expression of known ASCL1 downstream target genes including the SCLC oncogenes *SOX2* and *PROX1*, NOTCH pathway gene *RBPJ*, genes associated with neuronal signaling such as *SYT1, GRIP1, and TPH1*, and ion-channel encoding genes *SCN3A*, *KCNH8*, *KCNB2*, *KCNG3*, *and KCNA1* (17,46,62) (Figure 7G and H, Supplemental Table S3). In addition, the expression of other ASCL1 downstream targets including the SCLC oncogenes *RET, BCL2, NFIB* and *TRIT1,* NE markers *INSM1* and *NCAM1,* neural development genes *SOX11*, *NKX2-2*, and *FOXG-1*, and neuronal signaling genes *GABRB3*, *GRM8*, and *SNAP25,* among others, was on average lower in the INI-43-treated SCLC-A tumors, although these did not reach the 5% FDR criteria (Figure 7H, Supplemental Figure S5) (17,46,63). Expression of the full panel of previously identified ASCL1 downstream targets (17,46) in INI-43 versus vehicle-treated tumors is shown in Supplemental Figure S5. This decrease in ASCL1 downstream target expression is consistent with the reduced expression of ASCL1 downstream target genes observed following genetic depletion of KPNB1, or direct depletion of ASCL1 in SCLC-A cells *in vitro* (Figure 2E). Taken together, our findings suggest that reduced expression of known ASCL1 downstream

target genes may act in concert with disrupted cell cycle activity to produce the antitumor efficacy of INI-43 observed in the SCLC-A but not SCLC-N PDX model.

There are also genes uniquely upregulated in the INI-43-treated SCLC-A PDXs that encode proapoptotic proteins such as DIABLO (SMAC), BAX, TNFS10 (TRAIL), DAPK3, and TRADD, (Figure 7G and H), consistent with the apoptotic pathway enrichment observed in the INI-43-treated SCLC-A PDXs (Supplemental Table S3), and the growth inhibitory effect of INI-43 in this model. Consistently, Immunohistochemical (IHC) analysis of cleaved caspase-3 (CC3) revealed a higher percentage of CC3-expressing cells in the INI-43 versus vehicle-treated PDX samples, though this difference was not statistically significant (Supplemental Figure S6A, B).

Interestingly, the upregulated DEG unique to the INI-43-treated SCLC-A tumors were also enriched for the Reactome terms “Response to Metal Ions” and “Metallothioneins Bind Metals” (Figure 7G and H, Supplemental Table S3). A majority of the DEG associated with these pathways including the metallothioneins MT1E, MT1H, MT1F, MT1X, and MT2A have been shown to be markers of embryonic stem cells (ESCs) (64) or induced pluripotent stem cells (iPSCs) (65,66). In the ASCL1-regulated differentiation of iPSCs to neurons (65,67), neuronal differentiation is associated with increased ASCL1, and dramatically decreased MT1F and MT1X expression (65), suggesting that these genes may represent additional ASCL1 targets perturbed by indirect disruption of ASCL1 activity following KPNB1 inhibition.

KPNB1 inhibition in the SCLC RPM mouse model leads to downregulation of neuronal and developmental pathways

In addition to the PDX model, we also tested the ability of INI-43 to disrupt tumor growth in the RPM model, a MYC-driven SCLC GEMM (68). Here, SCLC-like tumors are generated by genetic deletion of tumor suppressors RB1 and TP53, combined with increased MYC in CGRP+ NE lineage cells in the lung. These tumors transition from ASCL1 to NEUROD1 to YAP1+ (58) and thus, different tumor samples express varying levels of ASCL1 and NEUROD1 (Supplemental Figure S7D, Supplemental Table S4) (58,68). INI-43 treatment in this model

resulted in no significant effect on survival or tumor growth (Supplemental Figure S7A,B). Furthermore, RNA-seq analysis of tumors from INI-43 treated RPM mice versus control mice was performed but revealed only 336 DEG in the NEUROD1^{High} tumors (n=4 INI-43, n=5 control) and 18 DEG (n=5 INI-43, n=4 control) in the ASCL1^{High} tumors. Nonetheless, INI-43-treatment in the NEUROD1^{High} tumors led to the downregulation of various neuronal and developmental pathways (Supplemental Figure S7F), and decreased expression of NEUROD1 SCLC target genes *SEMA6D*, *GNAO1*, *NCAM1, KCNK3, EBF1, NHLH1,* and *NHLH2 (17)*, and NEUROD1 pancreatic beta cell genes *KIF5C*, *SYT13*, and *GPX3* (69) (Supplemental Figure S7G, Supplemental Table S4). Given NEUROD1's established role in regulating neuronal and pancreatic beta cell differentiation during development (9,69), the downregulation of neuronal/developmental pathways combined with the reduction in NEUROD1 downstream target and pancreatic beta cell marker expression, suggests that *in vivo* KPNB1 inhibition may also disrupt NEUROD1 transcriptional activity in the RPM model, though this does not result in decreased tumor progression. Interestingly, treatment with INI-43 in the NEUROD1^{High} tumors also led to significant upregulation of *YAP1*. These findings are consistent with a model whereby loss of NEUROD1 in SCLC may lead to a YAP1+ state, either by inhibition of NEUROD1's nuclear import and subsequent transcriptional activity, or an alternative KPNB1-dependent mechanism.

DISCUSSION

Lineage TFs ASCL1 and NEUROD1 are expressed in a majority of SCLC, drive expression of SCLC oncogenes, command distinct transcriptional programs, and are required for maintaining SCLC growth *in vivo* and *in vitro* (6,17,21,22). Strategies to inhibit the activity of these oncogenic transcription factors may therefore represent a unique therapy for the predominant SCLC subtypes. Here, we identified a novel strategy to disrupt the transcriptional activity ASCL1 and NEUROD1, lineage oncogenes for which there are no known direct inhibitors, by exploiting

the subcellular localization required for their DNA binding and downstream target activation (11). We identified KPNB1, a nuclear transport receptor that is ubiquitously expressed in SCLC and physically interacts with ASCL1 and NEUROD1 in SCLC-A and SCLC-N human cell lines, as a nuclear import receptor for ASCL1 and NEUROD1 in this disease.

KPNB1 mediates the nuclear import of ASCL1 and NEUROD1 in SCLC

Pharmacologic, siRNA, and CRISPRi strategies to inhibit KPNB1 all led to significantly impaired nuclear accumulation of ASCL1 and NEUROD1 in SCLC-A and SCLC-N human cell lines, respectively. Despite the reduced nuclear ASCL1 observed following KPNB1 depletion, KPNB1-mediated import was found to be responsible for only about half the nuclear accumulation of ASCL1 in SCLC-A models. Though no other nuclear import receptors were identified as ASCL1 interactors by mass-spectrometry (46), the 25 kDA predicted size of ASCL1 is within range for diffusion through the nuclear pore complex, raising the possibility that some monomeric ASCL1 may also reach the nucleus by this route. However, the efficiency of this process decreases rapidly for molecules beyond a 30-60 kDA size (29,70). Furthermore, the nuclear translocation of NEUROD1 in neuronal cells predominantly occurs after heterodimerization with TCF3, the 67 kDA E-protein binding partner common to ASCL1, NEUROD1, and MYOD (30,31). Thus, ASCL1/TCF3 heterodimers may be imported into the nucleus by multiple mechanisms, 50% being KPNB1-dependent.

Strengthening the conclusion that nuclear localization of ASCL1 relies on KPNB1, KPNA2, an Importin-α adaptor that binds both KPNB1 and its cargo, was also identified as an ASCL1 interactor in the mass-spectrometry analysis. This finding contrasts with that reported for NEUROD1 in neuronal cell lines where NEUROD1 is imported into the nucleus by KPNB1 in an importin-α -independent manner (30,31). Inhibition of Importin-α/β 1 nuclear import may therefore provide an additional strategy to disrupt KPNB1-mediated nuclear import of ASCL1 alone. Furthermore, combining KPNB1 inhibitors with other inhibitors that decrease the

abundance of ASCL1 protein in SCLC, such as CDK2 inhibition (71), may provide a robust decrease of ASCL1 in those tumors where it functions as a lineage oncogene.

Consistent with the reduced nuclear ASCL1 and NEUROD1, KPNB1 depletion led to decreased expression of previously identified ASCL1 and NEUROD1 downstream target genes, including known SCLC oncogenes and NE markers. In SCLC-A cells, CRISPRi-mediated repression of KPNB1 led to a pattern of ASCL1 gene signature expression consistent with direct repression of ASCL1 activity within the same cell line. *In vivo*, KPNB1 inhibition in the SCLC-A PDX model also led to reduced expression of known ASCL1 downstream target genes including SCLC oncogenes, and genes involved in neuronal development and signaling. Nonetheless, expression of some genes was differentially affected by repression of KPNB1 versus ASCL1, possibly due to KPNB1's import of numerous cargoes aside from ASCL1 (27). Overall, these findings indicate that KPNB1-mediated nuclear import of ASCL1, and to a lesser extent NEUROD1, plays a role in regulating the expression of genes important for SCLC growth, oncogenic properties, and subtype-specific gene expression, and lends support to the inhibition of KPNB1 as a strategy to indirectly repress the transcriptional activity of ASCL1 in SCLC.

KPNB1 as an anti-tumor strategy in SCLC

KPNB1 inhibition has been pursued as an anti-tumor strategy in multiple cancers through its mitotic function, or other broad effects (27,32). In SCLC cells with a known dependence on lineage TFs such as ASCL1, KPNB1 inhibition may have the added ability to deprive tumors of lineage TF activity, and thus the expression of SCLC oncogenes activated by these TFs. In this study, *in vitro* inhibition of KPNB1 with INI-43 preferentially disrupted the growth of SCLC-A and SCLC-N cell lines compared to SCLC-P. Using KPNB1-independent ASCL1 or NEUROD1 in rescue experiments, we demonstrated that the impaired nuclear accumulation of ASCL1, but not NEUROD1, plays a substantial role in mediating this effect. This was also seen in *in vivo* experiments where INI-43 treatment disrupted tumor growth in an SCLC-A, but not an SCLC-N PDX model. In both the SCLC-A and SCLC-N PDXs, KPNB1

inhibition led to upregulation of numerous proteasomal and translation-associated genes including ribosomal subunits, a phenotype reported in preneoplastic precursors of SCLC following ectopic expression of MYCL (72). Targeting rRNA synthesis with an RNA polymerase I inhibitor decreased SCLC tumor growth (72), suggesting that RNA polymerase I inhibitor treatment may augment the antitumor efficacy of INI-43 in the SCLC PDXs. The disruption in proteostasis shared between both SCLC-A and -N PDX models is not sufficient to disrupt tumor growth. The decrease in tumor growth may require additional pathway disruption such as the upregulation of proapoptotic genes and downregulation of numerous cell cycle pathways uniquely detected in the INI-43 treated SCLC-A PDXs. In summary, the growth inhibitory effect of KPNB1 inhibition in the SCLC-A PDX model may arise from a combination of reduced expression of known ASCL1 downstream target genes observed in this model, and previously reported broad effects of KPNB1 inhibition in cancer cells, such as disrupted cell cycle activity (32) or proteostasis (61).

In the absence of agents to directly inhibit ASCL1 or NEUROD1 function, we identified a strategy to indirectly target these lineage TFs by disrupting their import into the nucleus. ASCL1 and NEUROD1, and related bHLH TFs such as ASCL2 and ATOH1, have been reported in multiple tumor types in addition to SCLC including neuroendocrine tumors in the prostate and thyroid, medulloblastoma, and colon cancer (73-76). Thus, a strategy to target a shared mechanism required for their activity, in this case nuclear import, may have value beyond SCLC.

ACKNOWLEDGEMENTS

We acknowledge discussions with the UT Southwestern SCLC community, particularly Drs. John Minna, Melanie Cobb, and David McFadden, as well as the nuclear import expertise of Dr. Yuh Min Chook. We thank Chaoying Liang (UTSW Microarray Core) for Next Generation Sequencing, Noelle Williams (Preclinical Pharmacology Core) for mouse pharmacokinetic analysis and assistance with compound formulation for *in vivo* delivery, and Terry Shih (Flow Cytometry Core) for outstanding technical advice and service. We also thank Trisha Savage for help with PDX implantation, John Minna, Luc Girard, Boning Gao, and Adi Gazdar (deceased) (U24CA213274) for their work on SCLC cell lines and lineage-defining TFs, and Charles Rudin and J.T. Poirier for providing SCLC PDXs. Funding for this project was provided by NCI F30 CA228314 to D.P.K., NCI U01CA213338 supporting J.E.J., a Career Development Award (NCI Spore Grant in Lung Cancer P50CA70907) to K.P., CPRIT Training Grant RP160157 to K.R., NCI U01-CA231844 and U24-CA213274 supporting T.G.O., and P30CA042014 to Huntsman Cancer Institute.

CONTRIBUTIONS

Study design: D.P.K.

Supervision and resources: J.E.J.

Data acquisition and analysis: D.P.K., K.P., K.E.R., N.S.W., S.P.C., T.G.O., K.B.S., S.J.W.

Cell lines: V.S.

Bioinformatic analysis: R.K.K.

Writing: D.P.K. and J.E.J.

Funding Acquisition: J.E.J., and D.P.K.

Figure 1

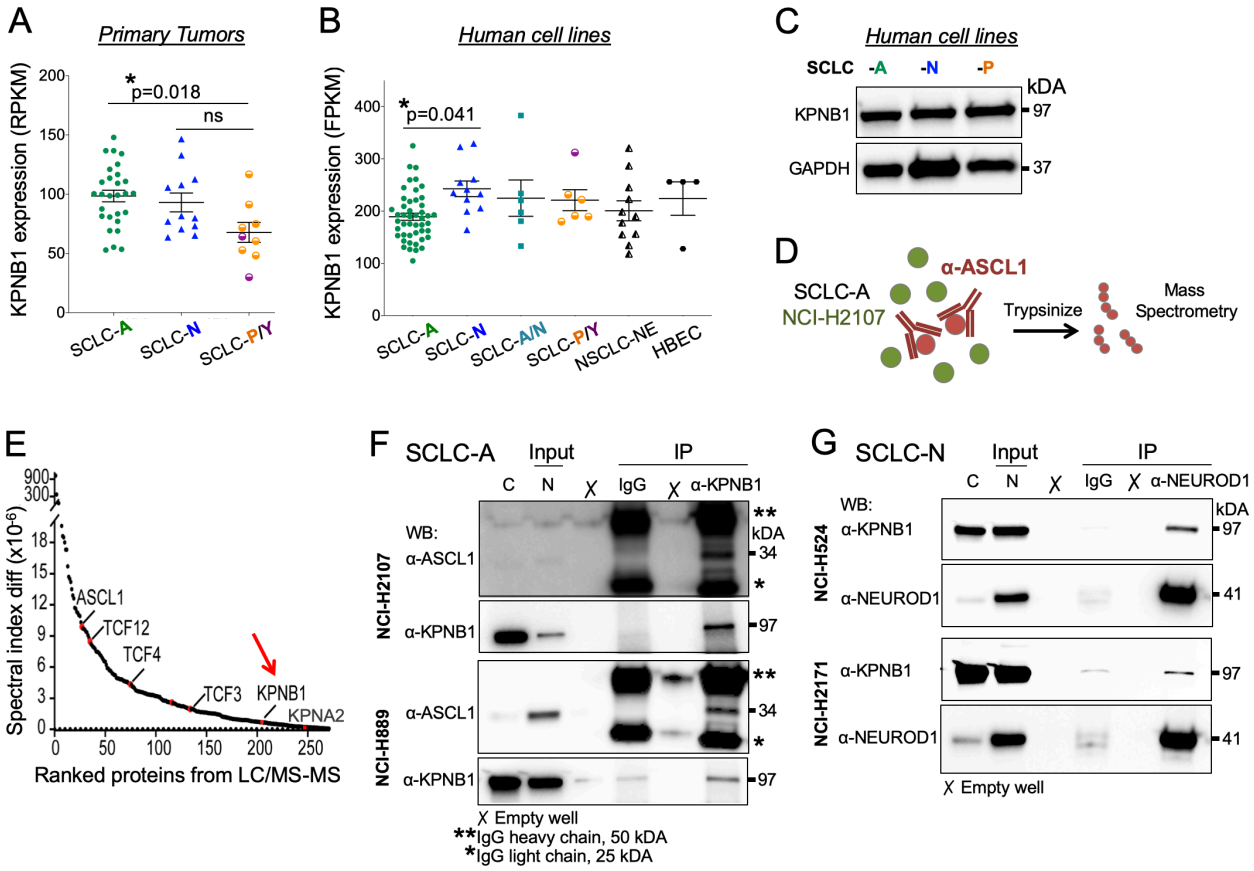

Figure 1. KPNB1 is highly expressed across SCLC models, and interacts with ASCL1 and NEUROD1 in human SCLC cell lines. (A) KPNB1 expression in SCLC-A (green), SCLC-N (blue), SCLC-P (orange) or SCLC-Y (purple) human primary tumors profiled by RNA-seq (5). Tumors were clustered into subtypes using SCLC-A, -N, or -P/Y classification. **(B)** KPNB1 expression in human SCLC-A, -N, -A/N, -P, or -Y cell lines, neuroendocrine NSCLC cell lines (NSCLC-NE), and immortalized human bronchial epithelial (HBEC) cell lines profiled by RNA-seq (center line, mean; whiskers, SEM; one-way ANOVA). **(C)** Western blot showing KPNB1 expression in representative SCLC-A, -N, or -P cell lines NCI-H2107, NCI-H2171, or NCI-H526 respectively. **(D)** Strategy for identifying ASCL1 binding partners in SCLC-A subtype NCI-H2107 cells by LC-MS/MS). **(E)** Proteins identified by mass spectrometry of ASCL1 immunoprecipitates shown ranked by spectral index. **(F)** Co-immunoprecipitation in combination with western blot

(co-IP/WB) demonstrating the interaction between KPNB1 and ASCL1 in SCLC-A cell lines NCI-H2107 and NCI-H889 (for NCI-H2107, input is 1% of protein loaded in IPs). **(G)** Co-IP/WB showing the interaction between NEUROD1 and KPNB1 in the SCLC-N cell lines NCI-H524 and NCI-H2171. C, cytoplasmic extract; N, nuclear extract. Nuclear extracts were used as IP input, non-immune IgG = IP control. *X* indicates wells with no lysate loaded.

Figure 2

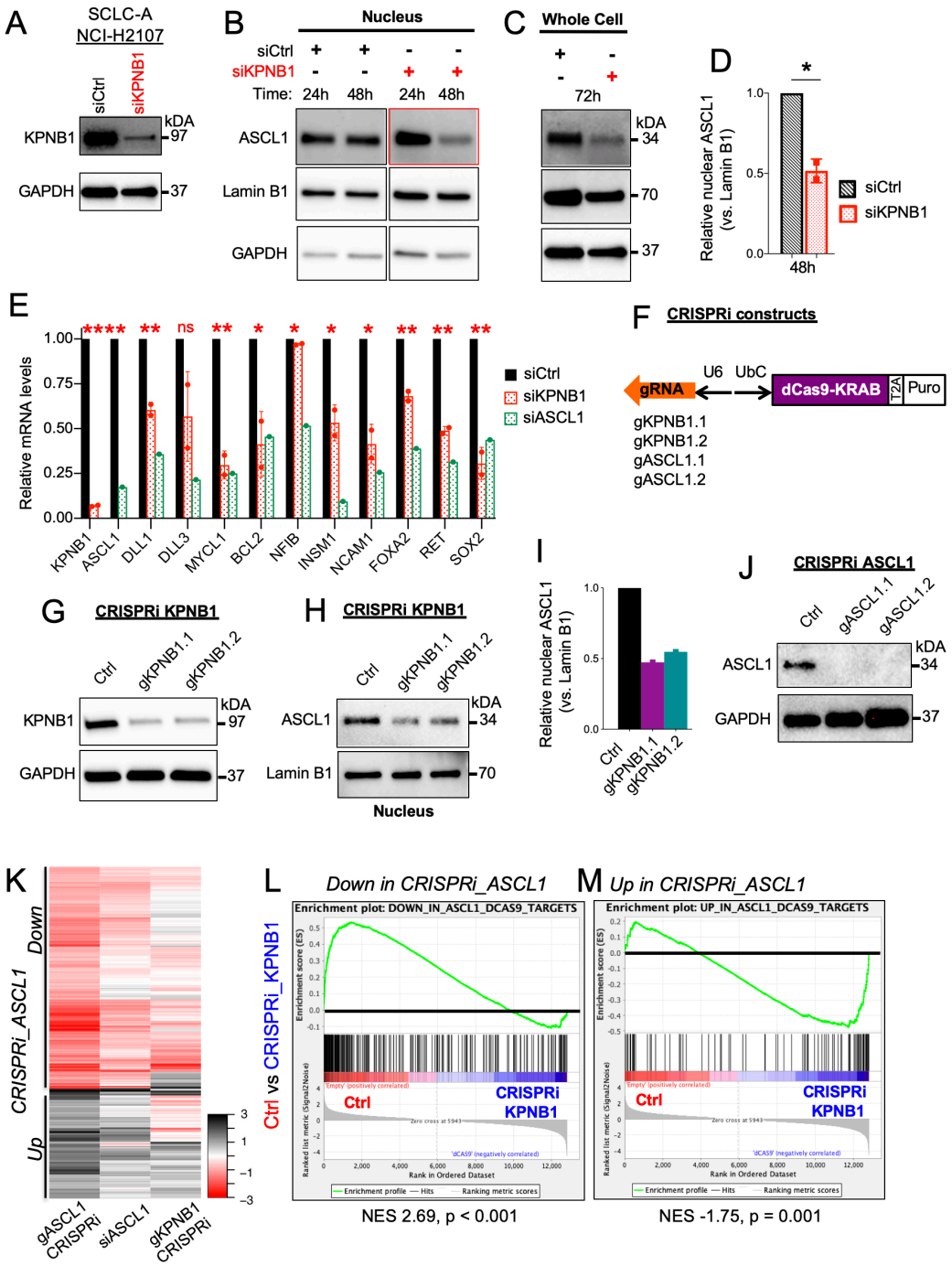

Figure 2. Depletion of KPNB1 reduces nuclear ASCL1, and ASCL1 downstream target gene expression in SCLC-A. (A) Western blot showing whole cell KPNB1 expression in SCLC-A subtype NCI-H2107 cells post-transfection with Control or KPNB1 siRNAs (siCtrl or

siKPNB1). **(B)** Western blots showing the level of ASCL1 in the nuclear, and whole cell lysate **(C)** fractions of NCI-H2107 cells at 24 and 48 hours post-siCtrl versus siKPNB1 transfection. **(D)** Quantification of relative ASCL1 protein in the nuclear fractions of siCtrl versus siKPNB1-transfected cells across two independent experiments. Lamin B1 = nuclear loading control (error bars, SEM; unpaired t-test). **(E)** Comparison of ASCL1 downstream target expression by RT-qPCR in siCtrl (black), siKPNB1 (red), and siASCL1 (green) transfected NCI-H2107 cells at 72 hours post-transfection. Average of three technical replicates from one experiment is shown (error bars, SEM, unpaired t-test,*$****p\leq 0.0001$,$***p\leq 0.001$,$**p\leq 0.01$,$*p\leq 0.05$). **(F)** Diagram of CRISPRi lentiviral construct where the UbC promoter drives expression of catalytically inactive Cas9 (dCas9) fused to the KRAB transcriptional repressor. U6 promoter drives expression of gRNAs targeting the 5'UTR of *KPNB1* (gKPNB1.1, gKPNB1.2) or *ASCL1* (gASCL1.1, gASCL1.2). **(G)** Expression of dCas9-KRAB plus gKPNB1.1 or gKPNB1.2 results in an 84% reduction in KPNB1 protein. **(H)** Western blot showing the level of ASCL1 in the nuclear fraction of NCI-H2107 cells expressing gKPNB1.1 or gKPNB1.2 versus Control (Ctrl). Quantification of nuclear ASCL1 protein is shown in **(I)**. **(J)** Western blot showing undetectable levels of ASCL1 in SCLC-A subtype NCI-H2107 cells expressing dCas9-KRAB plus ASCL1.1 or ASCL1.2 gRNAs. **(K)** Heatmap comparing expression of all DEG identified in CRISPRi_ASCL1 cells between siASCL1 knockdown NCI-H2107 cells previously profiled by RNA-seq (46) and CRISPRi_KPNB1 NCI-H2107 cell lines. Heatmap shows fold change of each gene with respect to each sample's control. **(L-M)** GSEA analysis from Ctrl versus CRISPRi_KPNB1 cell lines with normalized enrichment scores (NES) and p-values for all genes that were downregulated **(L)** or upregulated **(M)** following direct CRISPRi-mediated repression of ASCL1.

Figure 3

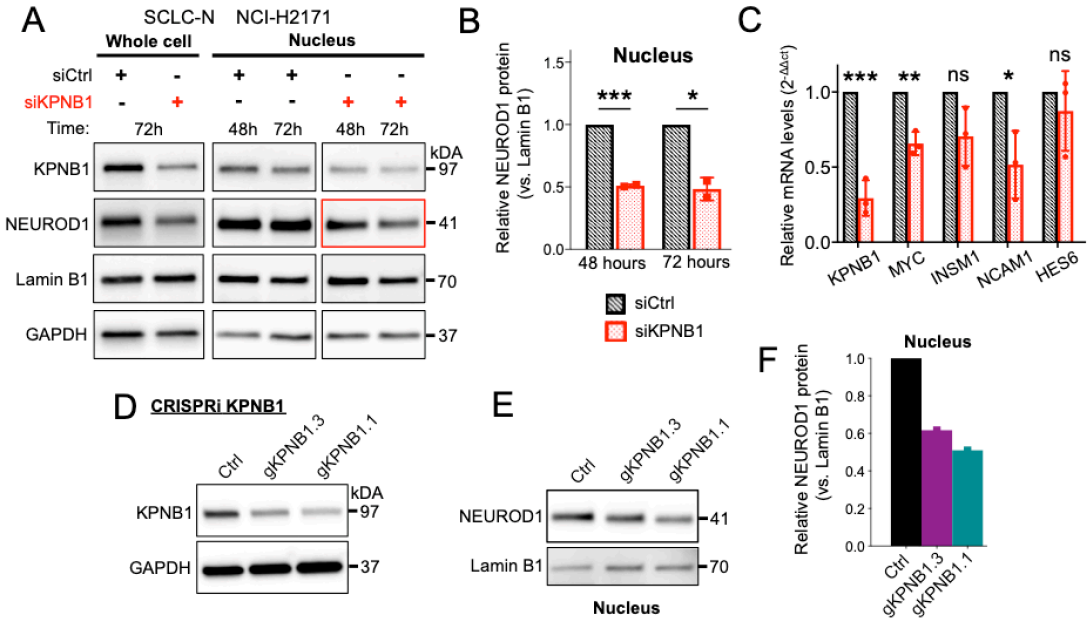

Figure 3. Depletion of KPNB1 reduces nuclear NEUROD1, and NEUROD1 downstream target expression in SCLC-N. (A) Western blots showing the level of KPNB1 and NEUROD1 in the nuclear and whole cell lysate fractions of SCLC-N subtype NCI-H2171 cells at 48 and 72 hours post-siCtrl versus siKPNB1 transfection. **(B)** Quantification of relative NEUROD1 protein in the nuclear fractions of siCtrl versus siKPNB1-transfected cells across two independent experiments (error bars, SEM; unpaired t-test). **(C)** Comparison of NEUROD1 downstream target expression in siCtrl versus siKPNB1-transfected NCI-H2171 cells at 72 hours post-transfection. Data points are average of three technical replicates from one independent experiment (error bars, SEM, unpaired t-test, ****p≤ 0.001, **p≤ 0.01, *p≤0.05*). **(D)** Expression of KPNB1.3 or KPNB1.1 gRNAs results in a 50-70% reduction in KPNB1 protein on western blot. **(E)** Western blot showing the level of NEUROD1 in the nuclear fraction of NCI-H2171 cells expressing KPNB1.3 or KPNB1.1 gRNAs versus Ctrl. Quantification of nuclear NEUROD1 protein is shown in **(F).**

Figure 4

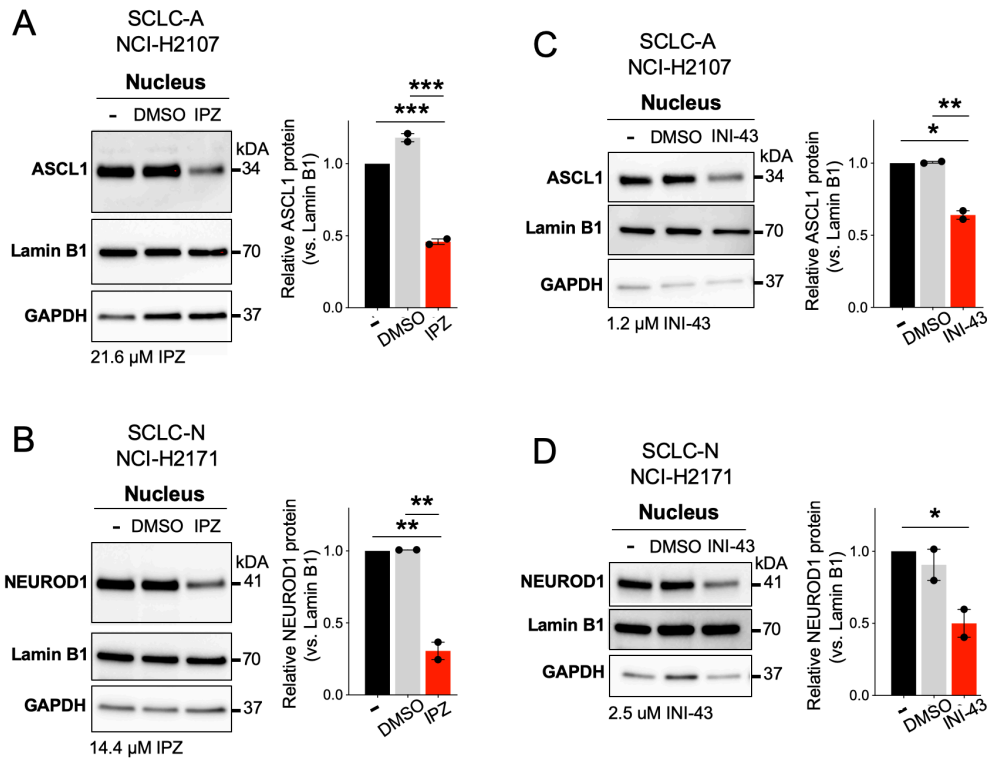

Figure 4. Pharmacologic inhibition of KPNB1 reduces nuclear ASCL1 and NEUROD1 in SCLC-A and SCLC-N. Western blots showing the levels of ASCL1 and NEUROD1 in the nuclear fractions **(A,C)** of SCLC-A subtype NCI-H2107 cells and **(B,D)** SCLC-N subtype NCI-H2171 cells treated with their respective IC50 concentrations of the KPNB1 inhibitors IPZ **(A,B)** or INI-43 **(C,D)** for 24 hours. Controls include the vehicle DMSO, and untreated (-) cells. Quantification of relative nuclear ASCL1 and NEUROD1 levels are shown next to each blot. Relative nuclear ASCL1 or NEUROD1 was quantified across two independent experiments (bars, mean ±SEM; one-way ANOVA, ***$p \leq 0.001$, **$p \leq 0.01$, *$p \leq 0.05$.).

Figure 5

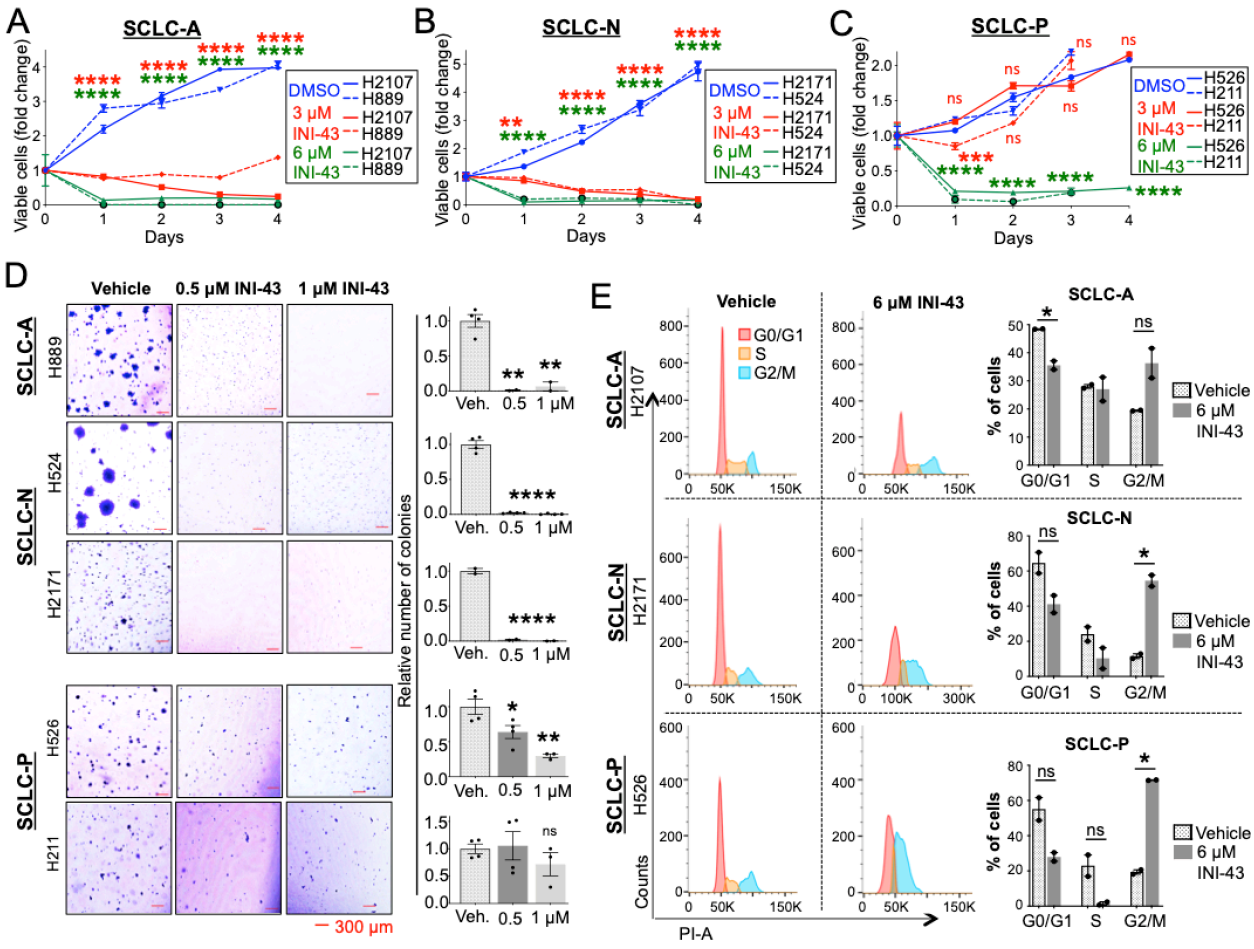

Figure 5. Pharmacologic inhibition of KPNB1 preferentially inhibits the growth of SCLC-A and SCLC-N relative to SCLC-P. Effect of 3 or 6 μM concentrations of INI-43 on the proliferation of SCLC-A subtype NCI-H2107 and NCI-H889 cell lines **(A)**, SCLC-N subtype NCI-H2171 and NCI-H524 cell lines **(B)**, and SCLC-P subtype NCI-H526 and NCI-H211 cell lines **(C)**. DMSO = vehicle. INI-43 was added to cell culture media at the time of plating. Cell viability was measured by WST-1 assay at the indicated timepoints post-plating (error bars, mean ±SEM; one-way ANOVA). **(D)** Representative images showing effect of 0.5 or 1 μM concentrations of INI-43 on the colony formation of SCLC-A, SCLC-N, and SCLC-P cell lines in soft agar. Quantification of colonies formed is shown to the right of the respective images (error bars, mean ±SEM; one-way ANOVA). **(E)** Cell cycle analysis was performed on SCLC-A,

SCLC-N, and SCLC-P cell lines treated with 6 μM INI-43 for 6 hours (error bars, mean ±SEM of two independent experiments; unpaired t-test, *****p*≤ *0.0001,*****p*≤ *0.001,**p*≤ *0.01,*p*≤ *0.05*).

Figure 6

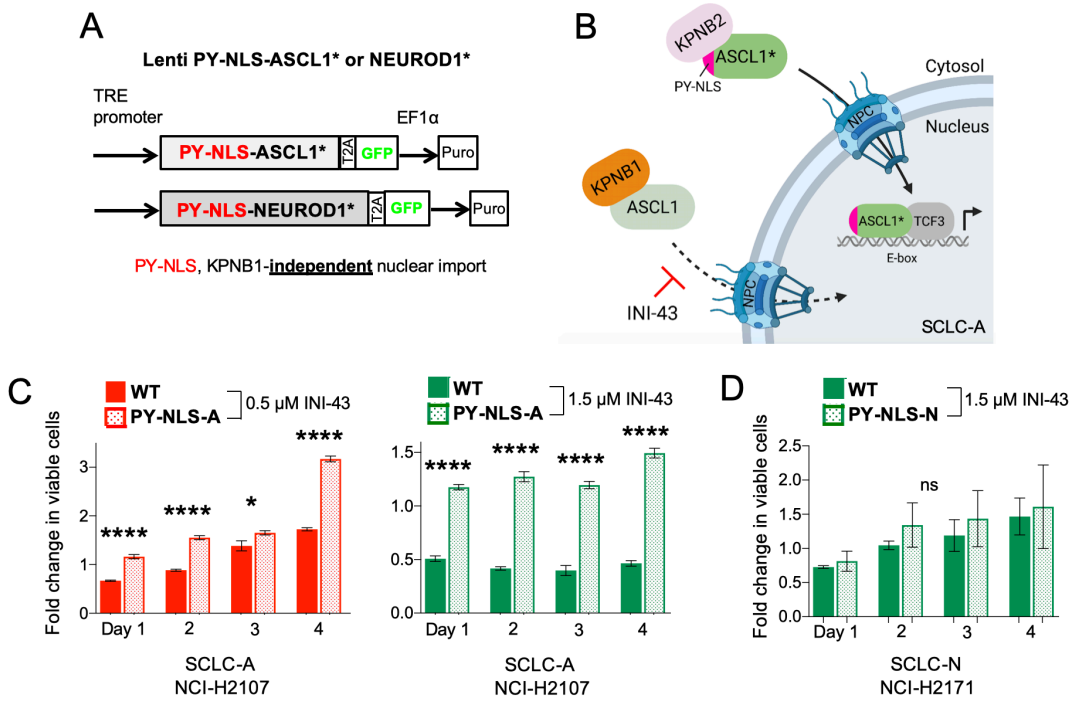

Figure 6. KPNB1-independent nuclear accumulation of ASCL1 rescues SCLC-A growth following KPNB1 inhibition. (A) Diagram of rescue constructs. Dox-inducible TRE promoter drives expression of ASCL1 and NEUROD1 variants with mutations in their putative NLS's (*), and a KPNB1-independent (KPNB**2**-specific) PY-NLS added to their N-termini. Wild type (WT) ASCL1 and NEUROD1 constructs serve as controls. **(B)** Rescue strategy. In SCLC-A cells, INI-43 inhibits KPNB1-mediated nuclear import of WT-ASCL1, but not KPNB2-specific PY-NLS-ASCL1*. In SCLC-N cells, the respective WT and PY-NLS-NEUROD1* constructs were used. **(C)** Comparison of the fold change in viable cells between the WT-ASCL1 or PY-NLS-ASCL1*-expressing SCLC-A subtype NCI-H2107 cell lines at 1 through 4 days post-treatment with 0.5 μM (red) and 1.5 μM (green) concentrations of INI-43. **(D)** Comparison of fold change in viable cells between WT-NEUROD1 or PY-NLS-NEUROD1*-expressing SCLC-N subtype NCI-H2171 cell lines at 1 through 4 days post-treatment with 1.5 μM INI-43. Cell viability was measured by

WST-1 assay (error bars, mean ±SEM of experiments performed in quintuplicate; unpaired t-test; second independent experiment confirmed results,****p≤ 0.0001,*p≤0.05).

Figure 7

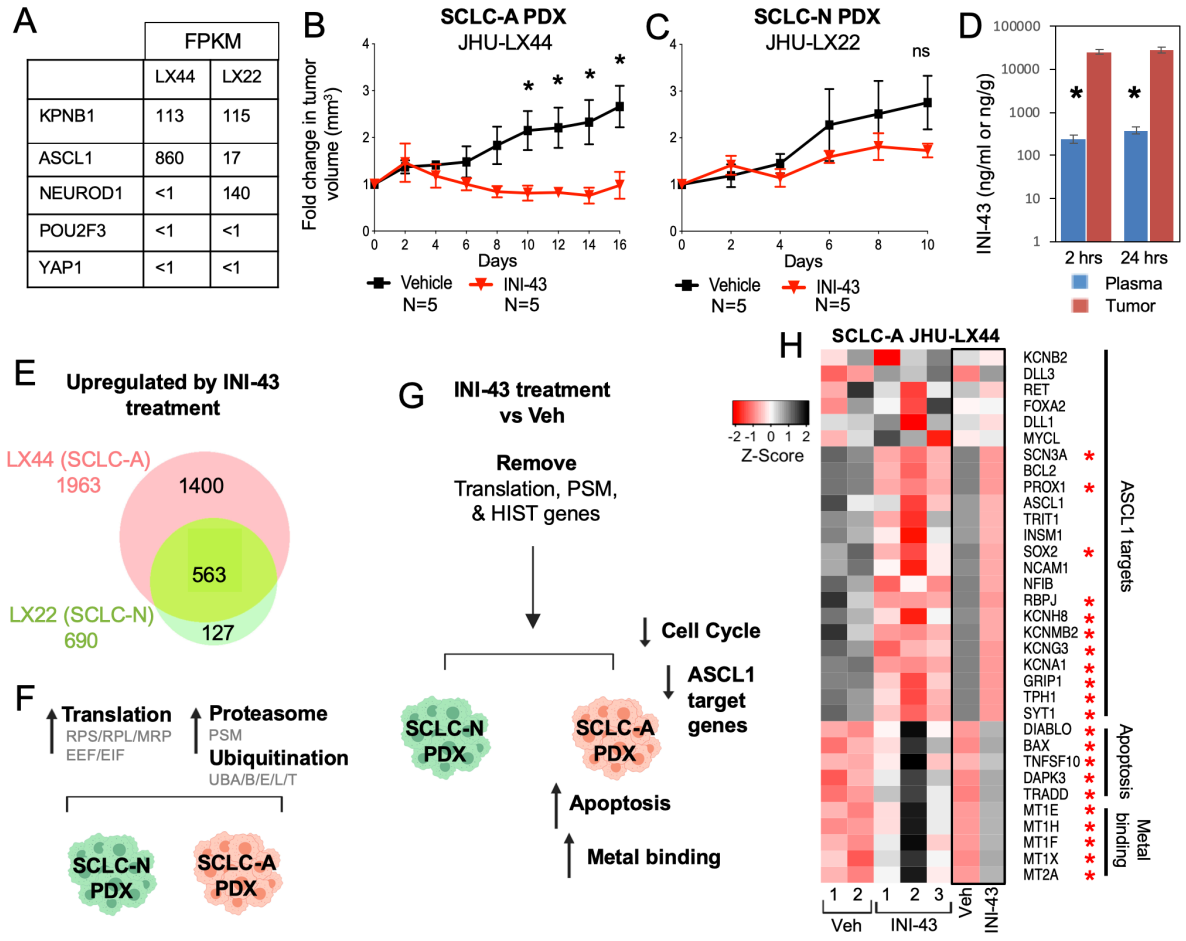

Figure 7. Pharmacologic inhibition of KPNB1 disrupts SCLC-A PDX growth *in vivo*. (A) FPKM expression values of KPNB1, ASCL1, NEUROD1, POU2F3, and YAP1 in JHU-LX44 and JHU-LX22 PDX samples profiled by RNA-seq. **(B-C)** Comparison of tumor growth in **(B)** SCLC-A (JHU-LX44) and **(C)** SCLC-N (JHU-LX22) PDX-bearing mice dosed with 25 mg/kg INI-43 versus vehicle for 10-16 days (n=5 per group). **(D)** LC-MS/MS analysis of INI-43 concentrations in plasma versus JHU-LX44 tumor tissue of INI-43 treated mice at 2 and 24 hours post-treatment (n=2 per group, per timepoint) (error bars, mean ±SD,*p≤0.05). **(E)** Venn diagram showing overlap in upregulated DEG identified following INI-43 treatment in the SCLC-A (pink) versus SCLC-N (green) PDX models. **(F)** In both models, INI-43 treatment leads to extensive upregulation of translation (RPS/RPL/MRP, EEF/EIF), histone (HIST), proteasomal (PSM), and

ubiquitin (UBA/B/E/L/T) genes. **(G)** Excluding translation, histone, and proteasomal genes, DEG uniquely identified in the INI-43-treated SCLC-A PDX samples revealed significant depletion of cell cycle pathways and decreased expression of ASCL1 downstream target genes. The expression of genes encoding proapoptotic proteins and metallothioneins shown in (H), was also uniquely elevated in the INI-43-treated SCLC-A PDXs. **(H)** Relative expression of select previously identified ASCL1 downstream targets, apoptotic and metallothionein genes in vehicle (n=2) versus INI-43-treated tumors (n=3) profiled by RNA-seq. Genes with significantly reduced, or increased expression at the 5% FDR criteria are indicated with a red or black asterisk, respectively. Average expression of these genes in the vehicle versus INI-43-treated samples is shown on the right.

METHODS

Cell lines and culture

Human SCLC cell lines used were NCI-H2107, NCI-H889, NCI-H2171, NCI-H524, NCI-H526, and NCI-H211 (Hamon Cancer Center, UT Southwestern). Cell lines were authenticated by DNA-fingerprinting (PowerPlex® 1.2 Kit, Promega #DC6500), tested for mycoplasma (e-Myco Mycoplasma PCR Detection Kit, Boca Scientific #25235), and cultured in RPMI-1640 Medium (ThermoFisher #11875135) supplemented with 10% FBS (GeminiBio #900-108) at 37°C in a humidified incubator with 5% CO_2.

Co-immunoprecipitation

Nuclear fractions from $4X10^6$ NCI-H2107, NCI-H889, NCI-H524, or NCI-H2171 cells were prepared (NE-PERTM Nuclear and Cytoplasmic Extraction kit, ThermoFisher #78835). 100 µg nuclear protein lysates from NCI-H2107 and NCI-H889 cells were incubated overnight (4°C) with 5 µg mouse anti-KPNB1 antibody (Santa Cruz #sc-137016) and NCI-H524 and NCI-H2171 lysates were incubated with 5 µg rabbit anti-NEUROD1 antibody (Abcam #ab109224). Normal mouse or rabbit IgG antibodies (Santa Cruz #sc-2025; Cell Signaling Technology #2729S) were used as respective controls. Immunoprecipitates were incubated for 90 minutes (4°C) with 70 µL Pierce™ Protein G Agarose beads (ThermoFisher #20397), washed in PBS containing 1% Triton-X100, eluted in Laemmli buffer, and resolved on 4–15% Mini- PROTEAN® TGX Stain-FreeTM Protein Gels (Bio-Rad), transferred to PVDF membranes, and probed with mouse anti-ASCL1 antibody (1:1000, BD Biosciences #556604) or mouse anti-KPNB1 antibody (1:1000, Santa Cruz #sc-137016), respectively, followed by HRP-conjugated anti-mouse secondary antibody (1:10000, Invitrogen #31432) or HRP-conjugated Trueblot® anti-rabbit secondary antibody (1:1000, Rockland #18-8816-33).

siRNA transfection

Cells were plated at $2X10^5$ cells/mL one day prior to transfection, and then resuspended, transferred to 12 well plates, and transfected by dropwise addition of a mixture containing 20 µL

X-tremeGENE™ siRNA Transfection Reagent (Sigma-Aldrich #4476115001), 500 nM siRNA, and 175 µL Opti-MEM™ (Gibco #31985062). siRNAs used were: Control siRNA-A (Santa Cruz #sc-37007), Karyopherin β1 siRNA(h) (Santa Cruz #sc-35736), and ASCL1 siRNA (ThermoFisher #HSS100744). For rescue experiments, ResKPNB1 vs. Vector Control expression was induced with 1 µg/mL doxycycline 24 hours prior to siRNA transfection and maintained by addition of 1 µg/mL doxycycline every 48 hours.

Western blotting

Nuclear and cytoplasmic protein fractionation was performed using the NE-PER™ Nuclear and Cytoplasmic Extraction kit (ThermoFisher #78835). Whole cell lysate samples were prepared in RIPA buffer plus protease and phosphatase inhibitors (ThermoFisher #78441). Protein content was quantified by Pierce™ BCA Protein Assay (ThermoFisher #23225). Samples were separated on 4–15% Mini-PROTEAN® TGX Stain-Free™ Protein Gels (Bio-Rad) after heat denaturation in Laemmli buffer. Proteins were transferred to Immobilon-P PVDF membranes (Millipore #IPVH00010). Membranes were blocked in 5% nonfat milk in TBS-T, probed with primary antibodies overnight (4°C), and incubated with HRP-conjugated secondary antibodies for 2 hours at room temperature. Proteins were detected using SuperSignal™ West Pico PLUS Chemiluminescent Substrate (ThermoFisher Scientific #34580). Membranes were imaged using a ChemiDoc Imaging System (Bio-Rad) and quantified using Image Lab™.

Antibodies

The antibodies used were: mouse anti-ASCL1 (1:1000, BD Biosciences #556604); rabbit anti-NEUROD1 (1:1000, Abcam #ab109224); mouse anti-KPNB1 (1:1000, Santa Cruz #sc-137016); rabbit anti-SOX9 (1:1000, Abcam #ab185966); rabbit anti-Lamin B1 (1:1000, Abcam #ab65986); mouse anti-GAPDH (1:1000, Santa Cruz #sc-47724). Secondary antibodies were: HRP-conjugated Goat anti-Rabbit IgG (H+L) (1:10000, Invitrogen #31462); HRP-conjugated Goat anti-Mouse IgG (H+L) (1:10000, Invitrogen #31432), and HRP-conjugated Trueblot® anti-rabbit (1:1000, Rockland #18-8816-33).

RT-qPCR

Cells were harvested by centrifugation and resuspended in TRIzol™ (Thermofisher #15596026). RNA was extracted using PicoPure™ RNA Isolation Kit (ThermoFisher #KIT0204). Tumor tissue was homogenized in TRIzol™ and total RNA was extracted using a Direct-zol RNA Miniprep kit (Zymo #R2052). cDNA was synthesized using SuperScript™ III First-Strand Synthesis SuperMix (Invitrogen # 11752050). RT-qPCR was performed on Applied Biosystems®7500 Fast thermocycler using Fast SYBR™ Green MasterMix (Applied Biosystems® #4385612). Reactions were performed in triplicate. Primer sequences are in Supplemental Table S1.

Plasmids

Guides, and cloned coding sequences are in Supplemental Table S1. Constructs used were generated as follows:

Lenti gRNA-dCas9-KRAB

gRNAs were synthesized (IDT-DNA), annealed, phosphorylated, and inserted into the Lenti dCas9-KRAB backbone using BsmBI sites (pLV hU6-sgRNA hUbC-dCas9-KRAB-T2a-Puro was a gift from Charles Gersbach; Addgene plasmid #71236; http://n2t.net/addgene:71236; RRID:Addgene_71236).

Lenti siRNA-Resistant KPNB1

A gene fragment encoding the KPNB1 protein coding region was made resistant to siRNA targeting by introduction of silent mutations at all sequences targeted by the commercial KPNB1 siRNAs used (Karyopherin β1 siRNA(h) (Santa Cruz #sc-35736). The gene fragment was synthesized (GenScript) and inserted into the TLCV2 backbone in place of Cas9 using AgeI and BamHI sites (TLCV2 was a gift from Adam Karpf; Addgene plasmid #87360; http://n2t.net/addgene:87360 ; RRID:Addgene_87360).

Lenti PY-NLS-ASCL1/NEUROD1*-FLAG*

Gene fragments encoding ASCL1 or NEUROD1 protein coding regions were designed with the following modifications: all basic amino acids in the putative NLS's of both proteins were mutated to alanine, the PY-NLS sequence from the KPNB2-specific RNA binding protein hnRNP M was added to the N-termini, and a FLAG-tag was added to the C-termini. Wildtype ASCL1-FLAG and NEUROD1-FLAG were used as controls. Coding regions were synthesized (GenScript) and inserted into the TLCV2 backbone as described above. For rescue, construct expression was induced with 1 µg/mL doxycycline at the time of INI-43 treatment. The FLAG-tag was not detected so the nuclear levels of the exogenous plus endogenous TFs were detected with antibodies to ASCL1 or NEUROD1.

Lentivirus production and generation of stable cell lines

5 µg transfer plasmid, 1 µg pCMV-VSV-G (Cell Biolabs #VPK-206), and 3 µg psPAX2 (Addgene #12260) were transfected into HEK293T cells using X-tremeGENE^{TM} HP DNA Transfection Reagent (Roche #6366236001). Viral supernatants were collected 48 hours post-transfection, filtered through a 0.45 µM filter, and added to NCI-H2107 and NCI-H2171 cells. Cells were incubated with virus for 48 hours and 1µg/mL puromycin containing RPMI-10% FBS media was used to select for cells expressing lentiviral inserts. Cells were maintained in RPMI-10% FBS supplemented with 0.1 µg/mL puromycin.

Cell viability assays

Cell viability was measured using the WST-1 Cell Proliferation Reagent (Roche #11644807001). Cells treated with siRNAs or KPNB1 inhibitors were resuspended and transferred to 96 well plates. 10 µL WST-1 reagent was added/well and plates were incubated for 2 hours (37°C) in a humidified incubator containing 5% CO_2. Absorbance was read using a multi-well plate reader.

For IC50 determinations, cells were plated at 2X10^5 cells/mL in 12-well plates and treated with IPZ or INI-43 for 24 hours (Supplemental Figure S3). Cell viability was measured by WST-1 assay as described. Experiments were performed in quintuplicate and IC50s were calculated as the average IC50 between two or three independent experiments.

Chemical compounds

Inhibitor of Nuclear Import-43 (INI-43) (Sigma-Aldrich #SML1911) and Importazole (IPZ) (Sigma-Aldrich #SML0341) were dissolved in DMSO to stock concentrations of 25 mM and 50 mM, respectively for *in vitro* experiments. For *in vivo* studies, INI-43 was dissolved in 10% DMSO/20% PEG400/70% PBS.

Soft agar assays

Cells were seeded at 20,000 cells/well in 12-well plates in a layer of 0.32% agar (SeaKem® LE Agarose (Lonza #50000)/RPMI/FBS/0.64% Antibiotic-Antimycotic (Gibco #15240-096) over a layer od 0.5% agar/RPMI/FBS/0.64% Antibiotic-Antimycotic. Cells were treated with vehicle or INI-43 at 0.5, 1, or 2 µM concentrations in the top agar layer at the time of plating. Cultures were grown for 3 weeks at 37°C in a humidified incubator containing 5% CO_2. Colonies were fixed and stained with 14.3% ethanol and 0.1% crystal violet in water. Plates were imaged using a Keyence BZ-X700 Series microscope (2X magnification, Z-stack, 25.2 µm pitch), and colonies quantified using the BZ-X700 Analysis software, where the Hybrid Cell Count feature was used to define the minimum colony area for each cell line.

Cell cycle analysis

Cells were plated at $2X10^5$ cells/mL, treated with 3 or 6 µM concentrations of INI-43, or vehicle, for 6 hours, harvested by centrifugation, fixed in ethanol at 4°C overnight, and stained with a solution containing 0.1% Triton X-100 in PBS, 0.2 mg/mL DNAse-free RNAse A (Sigma #R4642), and 0.2 mg/mL PI (Sigma #P4170) at 37°C for 15 minutes in the dark. DNA content of the stained cells was analyzed on a BD FACSLyric™ flow cytometer. Histograms of cell cycle distribution were generated from 10,000 events/sample. Raw data was analyzed using FlowJo 10.7.0.

INI-43 treatment in PDX models

PDX models JHU-LX44 and JHU-LX22 were established using dissociated cells from resected PDX tumors (gifted from C. Rudin and J.T. Poirier, Memorial Sloan Kettering, NYC). Tumors were engrafted by subcutaneous injection of $1X10^6$ JHU-LX44 cells or $2.4\ X10^6$ JHU-LX22 cells resuspended 1:1 in Matrigel (BD Biosciences #354234) and HITES media into the flanks of NSG mice. INI-43 treatment was initiated at a xenograft volume of ~500 mm^3 in JHU-LX44 mice (n=5 vehicle, n=5 INI-43), and ~600 mm^3 in JHU-LX22 tumor mice (n=5 vehicle, n=5 INI-43). Mice were intraperitoneally injected every 2 days with Vehicle (10% DMSO/20% PEG400/70% PBS) or 25 mg/kg INI-43 for 2 weeks or 10 days, respectively. Tumors were measured every 2 days with an external caliper. Tumor volume was calculated as described (77). Mice were sacrificed on the last day of treatment by CO_2 asphyxiation. Tumor tissue was harvested and processed as described. Mice were housed and treated according to regulations set by the IACUC of UT Southwestern Medical Center.

INI-43 pharmacokinetic analysis

JHU-LX44 tumor bearing mice were dosed with vehicle or 25 mg/kg INI-43 and animals were euthanized by inhalation overdose of CO_2 in groups of 2 at 24 hours post-dose. Blood was collected by cardiac puncture using an acidified citrate dextrose (ACD)-coated syringe, and plasma was isolated from whole-blood by centrifugation. Tumors were harvested, washed in PBS to remove residual circulating blood, flash-frozen in liquid nitrogen, and homogenized in 3X volume of PBS. Plasma and tumor levels of INI-43 were measured by LC-MS/MS as described (78).

Immunohistochemistry (IHC)

Tissues were fixed in 10% neutral buffered formalin for 24 hours on a shaker (4°C), and washed and stored in PBS (4°C) until embedding. Paraffin embedding was performed by the UT Southwestern Molecular Pathology Core. FFPE tissue blocks were incubated in room temperature water for 2 minutes and then ice cold water for 2 minutes before sectioning.

Tissues were cut at 5-μm sections using a Leitz 1512 Rotary Microtome. Sections were transferred to positively charged slides (Fischer Scientific #12-550-15) and allowed to dry overnight. Slides were warmed for 20 minutes in a 60°C oven before deparaffinization, deparaffinized with xylene, rehydrated with deionized water, and subjected to immunohistochemical (IHC) analysis using for Ki67 (Abcam #ab15580), and CC3 (Cell Signaling #9664): following antigen retrieval with citrate buffer and inhibition of endogenous peroxidase activity with 5% H_2O_2, slides were incubated with 5% normal goat serum for 1 hour at room temperature. Sections were incubated with primary antibody overnight (4°C), and then incubated with HRP-conjugated secondary antibody (Vector Laboratories) for 1 hour at room temperature followed by development using chromogenic substrate DAB for 10 minutes at room temperature. Slides were imaged using a NanoZoomer (Hamamatsu), and antibody staining quantification was performed using Fiji software. The same intensity threshold was used for a specific antibody staining. Images were then deconvoluted to binary format. The area fraction of the DAB signal in the resulting binary images was calculated and normalized to hematoxylin nuclear stain.

INI-43 treatment in RPM model

Anesthetized 6-8 week old RPM mice ($Rb1^{fl/fl}$;$p53^{fl/fl}$;$MycT58A^{LSL/LSL}$) (JAX:029971) were infected intranasally with $1x10^8$ plaque-forming units of Ad5-CGRP-Cre as described (58,68). INI-43 treatment was initiated at the earliest signs of tumor burden (~10% tumor volume/lung volume) determined by microCT imaging as described (58). Mice were treated with Vehicle (n=15), or 25 mg/kg INI-43 (n=8) every 3 days for 9-15 days. For chemotherapy (n=18), mice were treated with 5mg/kg cisplatin (Sigma #P4394) in PBS and 10mg/kg etoposide (Sigma #E1383) in 70% PEG in water on the following day. Drugs were administered by intraperitoneal injection once per week. Tumor burden was monitored by microCT (58,68). INI-43 cohorts were weighed daily to assess overall condition. Animals were sacrificed due to tumor burden. Tumor tissue was

harvested and processed as described. Mice were housed and treated according to regulations set by the IACUC of The University of Utah.

RNA-seq

Total RNA was extracted from cell pellets and SCLC tumor tissue as described above. RNA quality was checked by Bioanalyzer, and samples were submitted to the UTSW Genomics Sequencing & Microarray Core Facility for mRNAseq-Strand specific library preparation and sequencing of libraries using a NextSeq 500/550 High Output Kit v2.5 (75 Cycles) (Illumina #20024906), at 20-30 million reads/sample.

Bioinformatic analysis

Sample reads were aligned to the human genome using TopHat (v.2.1.2). Default settings were used, with the exception of –G, specifying assembly to the hg38 genome, --library- type fr -first strand, and –no-novel-juncs, which disregards noncanonical splice junctions when defining alignments. Cufflinks (v.2.2.2) was used to call and quantify transcripts from biological replicates for each sample, and identify differentially expressed genes (DEGs) between samples, using the default parameters. GO was performed with g:Profiler using the Reactome database and Benjamini-Hochberg Method to calculate FDR values. 5% FDR cutoff was used to select significantly enriched pathways. See Supplemental Table S3 for full details, DEG lists, and pathway analysis data.

To classify GEMM samples based on ASCL1 and NEUROD1 expression, we performed k-means clustering on all GEMM samples using pam() from cluster R package, and clustered the GEMM samples into three groups: $ASCL1^{High}$, $NEUROD1^{High}$ and dual-high (mixed). For differential expression analysis, we combined dual-high samples with both $ASCI1^{High}$ and $NEUROD1^{High}$ samples and called the DEGs. SW128 sample was not used as it has low levels of ASCL1 and NEUROD1.

Statistics

All other statistical analysis was performed using GraphPad Prism. Error bars show mean ± SEM and significance was determined by unpaired two tailed t-test with 95% confidence intervals or ordinary one-way ANOVA with multiple comparisons, unless otherwise specified, where $p<0.05$ was considered statistically significant. All other statistical details are described in respective figure legends.

Data and software

All RNA-seq data is deposited at GEO, and is publicly available (GSE185187). RNA-seq data from SCLC, NSCLC, and HBEC cell lines analyzed in this study is available in dbGaP (Study Accession phs001823.v1.p1). All additional data is available upon request. All software used is commercially available. Illustrations in Figures 6,7 were created with BioRender.com.

REFERENCES

1. Bunn PA, Jr., Minna JD, Augustyn A, Gazdar AF, Ouadah Y, Krasnow MA*, et al.* Small Cell Lung Cancer: Can Recent Advances in Biology and Molecular Biology Be Translated into Improved Outcomes? J Thorac Oncol **2016**;11:453-74
2. Gazdar AF, Bunn PA, Minna JD. Small-cell lung cancer: what we know, what we need to know and the path forward. Nat Rev Cancer **2017**;17:765
3. Ujhazy P, Lindwasser OW. Small cell lung cancer: updates and new concepts. Transl Lung Cancer Res **2018**;7:1-3
4. Peifer M, Fernandez-Cuesta L, Sos ML, George J, Seidel D, Kasper LH*, et al.* Integrative genome analyses identify key somatic driver mutations of small-cell lung cancer. Nat Genet **2012**;44:1104-10
5. George J, Lim JS, Jang SJ, Cun Y, Ozretic L, Kong G*, et al.* Comprehensive genomic profiles of small cell lung cancer. Nature **2015**;524:47-53
6. Rudin CM, Poirier JT, Byers LA, Dive C, Dowlati A, George J*, et al.* Molecular subtypes of small cell lung cancer: a synthesis of human and mouse model data. Nat Rev Cancer **2019**;19:289-97
7. Baine MK, Hsieh MS, Lai WV, Egger JV, Jungbluth AA, Daneshbod Y*, et al.* SCLC Subtypes Defined by ASCL1, NEUROD1, POU2F3, and YAP1: A Comprehensive Immunohistochemical and Histopathologic Characterization. J Thorac Oncol **2020**;15:1823-35
8. Johnson JE, Birren SJ, Anderson DJ. Two rat homologues of Drosophila achaete-scute specifically expressed in neuronal precursors. Nature **1990**;346:858-61
9. Lee JE, Hollenberg SM, Snider L, Turner DL, Lipnick N, Weintraub H. Conversion of Xenopus ectoderm into neurons by NeuroD, a basic helix-loop-helix protein. Science **1995**;268:836-44

10. Hevner RF, Hodge RD, Daza RA, Englund C. Transcription factors in glutamatergic neurogenesis: conserved programs in neocortex, cerebellum, and adult hippocampus. Neurosci Res **2006**;55:223-33
11. Bertrand N, Castro DS, Guillemot F. Proneural genes and the specification of neural cell types. Nat Rev Neurosci **2002**;3:517-30
12. Ito T, Udaka N, Yazawa T, Okudela K, Hayashi H, Sudo T*, et al.* Basic helix-loop-helix transcription factors regulate the neuroendocrine differentiation of fetal mouse pulmonary epithelium. Development **2000**;127:3913-21
13. Borges M, Linnoila RI, van de Velde HJ, Chen H, Nelkin BD, Mabry M*, et al.* An achaete-scute homologue essential for neuroendocrine differentiation in the lung. Nature **1997**;386:852-5
14. Meuwissen R, Linn SC, Linnoila RI, Zevenhoven J, Mooi WJ, Berns A. Induction of small cell lung cancer by somatic inactivation of both Trp53 and Rb1 in a conditional mouse model. Cancer Cell **2003**;4:181-9
15. Park KS, Liang MC, Raiser DM, Zamponi R, Roach RR, Curtis SJ*, et al.* Characterization of the cell of origin for small cell lung cancer. Cell Cycle **2011**;10:2806-15
16. Sutherland KD, Proost N, Brouns I, Adriaensen D, Song JY, Berns A. Cell of origin of small cell lung cancer: inactivation of Trp53 and Rb1 in distinct cell types of adult mouse lung. Cancer Cell **2011**;19:754-64
17. Borromeo MD, Savage TK, Kollipara RK, He M, Augustyn A, Osborne JK*, et al.* ASCL1 and NEUROD1 Reveal Heterogeneity in Pulmonary Neuroendocrine Tumors and Regulate Distinct Genetic Programs. Cell Rep **2016**;16:1259-72
18. Osada H, Tatematsu Y, Yatabe Y, Horio Y, Takahashi T. ASH1 gene is a specific therapeutic target for lung cancers with neuroendocrine features. Cancer Res **2005**;65:10680-5
19. Jiang T, Collins BJ, Jin N, Watkins DN, Brock MV, Matsui W*, et al.* Achaete-scute complex homologue 1 regulates tumor-initiating capacity in human small cell lung cancer. Cancer Res **2009**;69:845-54
20. Teicher BA. Targets in small cell lung cancer. Biochem Pharmacol **2014**;87:211-9
21. Augustyn A, Borromeo M, Wang T, Fujimoto J, Shao C, Dospoy PD*, et al.* ASCL1 is a lineage oncogene providing therapeutic targets for high-grade neuroendocrine lung cancers. Proc Natl Acad Sci U S A **2014**;111:14788-93
22. Osborne JK, Larsen JE, Shields MD, Gonzales JX, Shames DS, Sato M*, et al.* NeuroD1 regulates survival and migration of neuroendocrine lung carcinomas via signaling molecules TrkB and NCAM. Proc Natl Acad Sci U S A **2013**;110:6524-9
23. Henke RM, Meredith DM, Borromeo MD, Savage TK, Johnson JE. Ascl1 and Neurog2 form novel complexes and regulate Delta-like3 (Dll3) expression in the neural tube. Dev Biol **2009**;328:529-40
24. Massari ME, Murre C. Helix-loop-helix proteins: regulators of transcription in eucaryotic organisms. Mol Cell Biol **2000**;20:429-40
25. Gradwohl G, Fode C, Guillemot F. Restricted expression of a novel murine atonal-related bHLH protein in undifferentiated neural precursors. Dev Biol **1996**;180:227-41
26. Johnson JE, Birren SJ, Saito T, Anderson DJ. DNA binding and transcriptional regulatory activity of mammalian achaete-scute homologous (MASH) proteins

revealed by interaction with a muscle-specific enhancer. Proc Natl Acad Sci U S A **1992**;89:3596-600
27. Kosyna FK, Depping R. Controlling the Gatekeeper: Therapeutic Targeting of Nuclear Transport. Cells **2018**;7
28. Jamali T, Jamali Y, Mehrbod M, Mofrad MR. Nuclear pore complex: biochemistry and biophysics of nucleocytoplasmic transport in health and disease. Int Rev Cell Mol Biol **2011**;287:233-86
29. Timney BL, Raveh B, Mironska R, Trivedi JM, Kim SJ, Russel D*, et al.* Simple rules for passive diffusion through the nuclear pore complex. J Cell Biol **2016**;215:57-76
30. Mehmood R, Yasuhara N, Fukumoto M, Oe S, Tachibana T, Yoneda Y. Cross-talk between distinct nuclear import pathways enables efficient nuclear import of E47 in conjunction with its partner transcription factors. Mol Biol Cell **2011**;22:3715-24
31. Mehmood R, Yasuhara N, Oe S, Nagai M, Yoneda Y. Synergistic nuclear import of NeuroD1 and its partner transcription factor, E47, via heterodimerization. Exp Cell Res **2009**;315:1639-52
32. Cagatay T, Chook YM. Karyopherins in cancer. Curr Opin Cell Biol **2018**;52:30-42
33. Huenniger K, Kramer A, Soom M, Chang I, Kohler M, Depping R*, et al.* Notch1 signaling is mediated by importins alpha 3, 4, and 7. Cell Mol Life Sci **2010**;67:3187-96
34. Hill CS. Nucleocytoplasmic shuttling of Smad proteins. Cell Res **2009**;19:36-46
35. Yamasaki H, Sekimoto T, Ohkubo T, Douchi T, Nagata Y, Ozawa M*, et al.* Zinc finger domain of Snail functions as a nuclear localization signal for importin beta-mediated nuclear import pathway. Genes Cells **2005**;10:455-64
36. Stelma T, Leaner VD. KPNB1-mediated nuclear import is required for motility and inflammatory transcription factor activity in cervical cancer cells. Oncotarget **2017**;8:32833-47
37. Du W, Zhu J, Zeng Y, Liu T, Zhang Y, Cai T*, et al.* KPNB1-mediated nuclear translocation of PD-L1 promotes non-small cell lung cancer cell proliferation via the Gas6/MerTK signaling pathway. Cell Death Differ **2021**;28:1284-300
38. Forbes DJ, Travesa A, Nord MS, Bernis C. Nuclear transport factors: global regulation of mitosis. Curr Opin Cell Biol **2015**;35:78-90
39. Guttinger S, Laurell E, Kutay U. Orchestrating nuclear envelope disassembly and reassembly during mitosis. Nat Rev Mol Cell Biol **2009**;10:178-91
40. van der Watt PJ, Chi A, Stelma T, Stowell C, Strydom E, Carden S*, et al.* Targeting the Nuclear Import Receptor Kpnbeta1 as an Anticancer Therapeutic. Mol Cancer Ther **2016**;15:560-73
41. Yang J, Guo Y, Lu C, Zhang R, Wang Y, Luo L*, et al.* Inhibition of Karyopherin beta 1 suppresses prostate cancer growth. Oncogene **2019**;38:4700-14
42. Angus L, van der Watt PJ, Leaner VD. Inhibition of the nuclear transporter, Kpnbeta1, results in prolonged mitotic arrest and activation of the intrinsic apoptotic pathway in cervical cancer cells. Carcinogenesis **2014**;35:1121-31
43. Ha S, Choi J, Min NY, Lee KH, Ham SW. Inhibition of Importin beta1 With a 2-Aminothiazole Derivative Resulted in G2/M Cell-cycle Arrest and Apoptosis. Anticancer Res **2017**;37:2373-9

44. Farago AF, Yeap BY, Stanzione M, Hung YP, Heist RS, Marcoux JP, *et al.* Combination Olaparib and Temozolomide in Relapsed Small-Cell Lung Cancer. Cancer Discov **2019**;9:1372-87
45. Tlemsani C, Pongor L, Elloumi F, Girard L, Huffman KE, Roper N, *et al.* SCLC-CellMiner: A Resource for Small Cell Lung Cancer Cell Line Genomics and Pharmacology Based on Genomic Signatures. Cell Rep **2020**;33:108296
46. Pozo K, Kollipara RK, Kelenis DP, Rodarte KE, Ullrich MS, Zhang X, *et al.* ASCL1, NKX2-1, and PROX1 co-regulate subtype-specific genes in small-cell lung cancer. iScience **2021**;24:102953
47. Gillotin S, Davies JD, Philpott A. Subcellular localisation modulates ubiquitylation and degradation of Ascl1. Sci Rep **2018**;8:4625
48. Urban N, van den Berg DL, Forget A, Andersen J, Demmers JA, Hunt C, *et al.* Return to quiescence of mouse neural stem cells by degradation of a proactivation protein. Science **2016**;353:292-5
49. Nelson BR, Hartman BH, Ray CA, Hayashi T, Bermingham-McDonogh O, Reh TA. Acheate-scute like 1 (Ascl1) is required for normal delta-like (Dll) gene expression and notch signaling during retinal development. Dev Dyn **2009**;238:2163-78
50. Nelson BR, Reh TA. Relationship between Delta-like and proneural bHLH genes during chick retinal development. Dev Dyn **2008**;237:1565-80
51. Qi LS, Larson MH, Gilbert LA, Doudna JA, Weissman JS, Arkin AP, *et al.* Repurposing CRISPR as an RNA-guided platform for sequence-specific control of gene expression. Cell **2013**;152:1173-83
52. Gilbert LA, Larson MH, Morsut L, Liu Z, Brar GA, Torres SE, *et al.* CRISPR-mediated modular RNA-guided regulation of transcription in eukaryotes. Cell **2013**;154:442-51
53. Thakore PI, D'Ippolito AM, Song L, Safi A, Shivakumar NK, Kabadi AM, *et al.* Highly specific epigenome editing by CRISPR-Cas9 repressors for silencing of distal regulatory elements. Nat Methods **2015**;12:1143-9
54. Soderholm JF, Bird SL, Kalab P, Sampathkumar Y, Hasegawa K, Uehara-Bingen M, *et al.* Importazole, a small molecule inhibitor of the transport receptor importin-beta. ACS Chem Biol **2011**;6:700-8
55. Lee BJ, Cansizoglu AE, Suel KE, Louis TH, Zhang Z, Chook YM. Rules for nuclear localization sequence recognition by karyopherin beta 2. Cell **2006**;126:543-58
56. Soares MAF, Soares DS, Teixeira V, Heskol A, Bressan RB, Pollard SM, *et al.* Hierarchical reactivation of transcription during mitosis-to-G1 transition by Brn2 and Ascl1 in neural stem cells. Genes Dev **2021**;35:1020-34
57. Freeman BT, Sokolowski M, Roy-Engel AM, Smither ME, Belancio VP. Identification of charged amino acids required for nuclear localization of human L1 ORF1 protein. Mob DNA **2019**;10:20
58. Ireland AS, Micinski AM, Kastner DW, Guo B, Wait SJ, Spainhower KB, *et al.* MYC Drives Temporal Evolution of Small Cell Lung Cancer Subtypes by Reprogramming Neuroendocrine Fate. Cancer Cell **2020**;38:60-78 e12
59. Percharde M, Bulut-Karslioglu A, Ramalho-Santos M. Hypertranscription in Development, Stem Cells, and Regeneration. Dev Cell **2017**;40:9-21

60. Lavado A, Park JY, Pare J, Finkelstein D, Pan H, Xu B*, et al.* The Hippo Pathway Prevents YAP/TAZ-Driven Hypertranscription and Controls Neural Progenitor Number. Dev Cell **2018**;47:576-91 e8
61. Zhu ZC, Liu JW, Li K, Zheng J, Xiong ZQ. KPNB1 inhibition disrupts proteostasis and triggers unfolded protein response-mediated apoptosis in glioblastoma cells. Oncogene **2018**;37:2936-52
62. Zhu SH, Shan CJ, Wu ZF, Xu SZ. Proliferation of small cell lung cancer cell line reduced by knocking-down PROX1 via shRNA in lentivirus. Anticancer Res **2013**;33:3169-75
63. Coll-SanMartin L, Davalos V, Pineyro D, Rossello-Tortella M, Bueno-Costa A, Setien F*, et al.* Gene Amplification-Associated Overexpression of the Selenoprotein tRNA Enzyme TRIT1 Confers Sensitivity to Arsenic Trioxide in Small-Cell Lung Cancer. Cancers (Basel) **2021**;13
64. Pooyan P, Karamzadeh R, Mirzaei M, Meyfour A, Amirkhan A, Wu Y*, et al.* The Dynamic Proteome of Oligodendrocyte Lineage Differentiation Features Planar Cell Polarity and Macroautophagy Pathways. Gigascience **2020**;9
65. Lin M, Pedrosa E, Shah A, Hrabovsky A, Maqbool S, Zheng D*, et al.* RNA-Seq of human neurons derived from iPS cells reveals candidate long non-coding RNAs involved in neurogenesis and neuropsychiatric disorders. PLoS One **2011**;6:e23356
66. Kempf H, Olmer R, Kropp C, Ruckert M, Jara-Avaca M, Robles-Diaz D*, et al.* Controlling expansion and cardiomyogenic differentiation of human pluripotent stem cells in scalable suspension culture. Stem Cell Reports **2014**;3:1132-46
67. Vierbuchen T, Ostermeier A, Pang ZP, Kokubu Y, Sudhof TC, Wernig M. Direct conversion of fibroblasts to functional neurons by defined factors. Nature **2010**;463:1035-41
68. Mollaoglu G, Guthrie MR, Bohm S, Bragelmann J, Can I, Ballieu PM*, et al.* MYC Drives Progression of Small Cell Lung Cancer to a Variant Neuroendocrine Subtype with Vulnerability to Aurora Kinase Inhibition. Cancer Cell **2017**;31:270-85
69. Romer AI, Singer RA, Sui L, Egli D, Sussel L. Murine Perinatal beta-Cell Proliferation and the Differentiation of Human Stem Cell-Derived Insulin-Expressing Cells Require NEUROD1. Diabetes **2019**;68:2259-71
70. Ma J, Goryaynov A, Sarma A, Yang W. Self-regulated viscous channel in the nuclear pore complex. Proc Natl Acad Sci U S A **2012**;109:7326-31
71. Koduri V, Duplaquet L, Lampson BL, Wang AC, Sabet AH, Ishoey M*, et al.* Targeting oncoproteins with a positive selection assay for protein degraders. Sci Adv **2021**;7
72. Kim DW, Wu N, Kim YC, Cheng PF, Basom R, Kim D*, et al.* Genetic requirement for Mycl and efficacy of RNA Pol I inhibition in mouse models of small cell lung cancer. Genes Dev **2016**;30:1289-99
73. Cejas P, Xie Y, Font-Tello A, Lim K, Syamala S, Qiu X*, et al.* Subtype heterogeneity and epigenetic convergence in neuroendocrine prostate cancer. Nat Commun **2021**;12:5775
74. Chen H, Kunnimalaiyaan M, Van Gompel JJ. Medullary thyroid cancer: the functions of raf-1 and human achaete-scute homologue-1. Thyroid **2005**;15:511-21
75. Flora A, Klisch TJ, Schuster G, Zoghbi HY. Deletion of Atoh1 disrupts Sonic Hedgehog signaling in the developing cerebellum and prevents medulloblastoma. Science **2009**;326:1424-7

76. Jubb AM, Chalasani S, Frantz GD, Smits R, Grabsch HI, Kavi V*, et al.* Achaete-scute like 2 (ascl2) is a target of Wnt signalling and is upregulated in intestinal neoplasia. Oncogene **2006**;25:3445-57
77. Wang X-D, Hu R, Ding Q, Savage TK, Huffman KE, Williams N*, et al.* Subtype-specific secretomic characterization of pulmonary neuroendocrine tumor cells. Nature Communications **2019**;10:3201
78. Wang W, Zhang L, Morlock L, Williams NS, Shay JW, De Brabander JK. Design and Synthesis of TASIN Analogues Specifically Targeting Colorectal Cancer Cell Lines with Mutant Adenomatous Polyposis Coli (APC). J Med Chem **2019**;62:5217-41

Figure 1

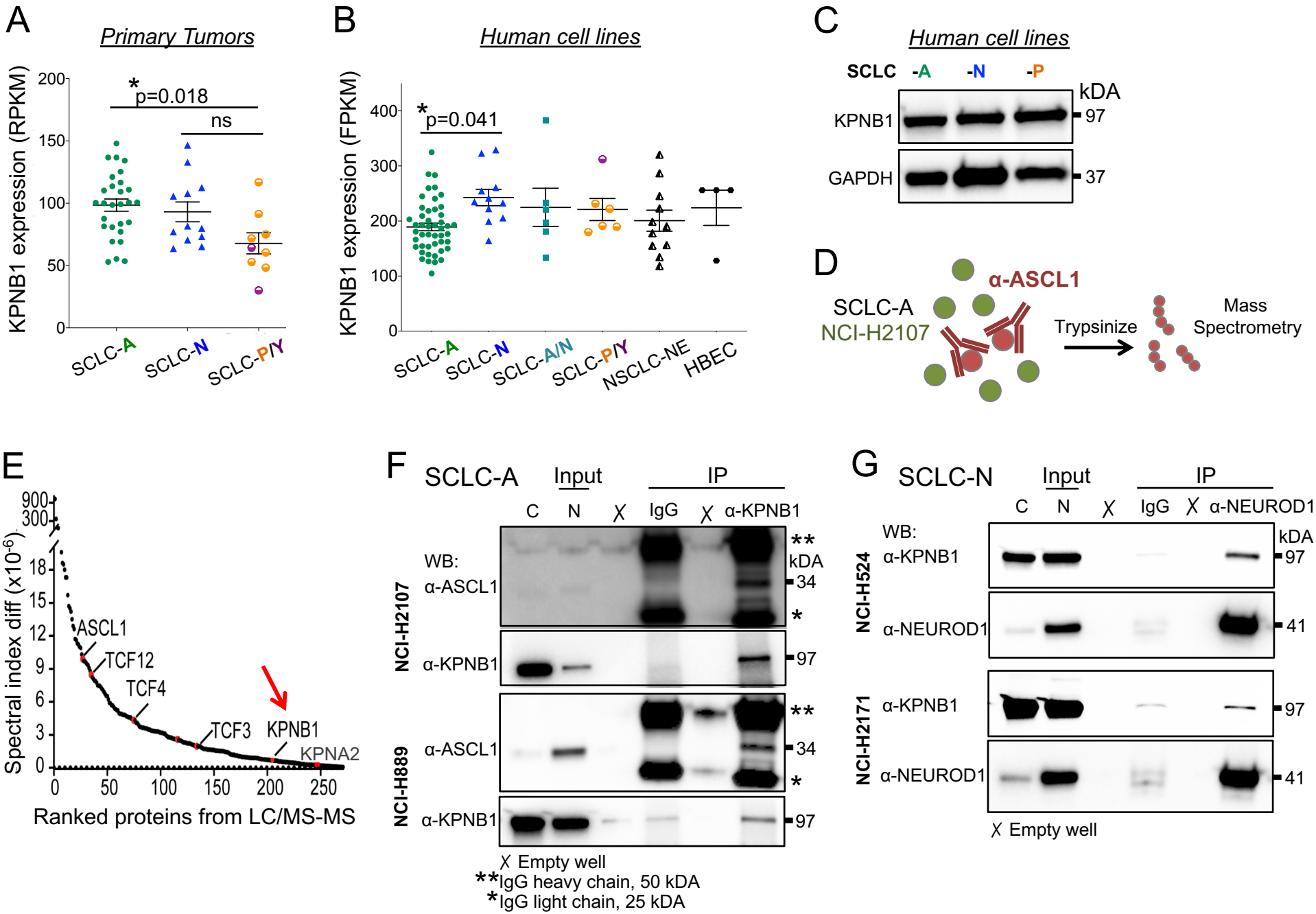
A
Primary Tumors
KPNB1 expression (RPKM)
*p=0.018
ns
SCLC-A
SCLC-N
SCLC-P/Y
B
Human cell lines
KPNB1 expression (FPKM)
*p=0.041
SCLC-A
SCLC-N
SCLC-A/N
SCLC-P/Y
NSCLC-NE
HBEC
C
Human cell lines
SCLC -A -N -P
kDA
KPNB1
97
GAPDH
37
D
α-ASCL1
SCLC-A
NCI-H2107
Trypsinize
Mass Spectrometry
E
Spectral index diff (x10-6)
ASCL1
TCF12
TCF4
TCF3
KPNB1
KPNA2
Ranked proteins from LC/MS-MS
F
SCLC-A
Input
IP
C N X IgG X α-KPNB1
WB:
α-ASCL1
α-KPNB1
NCI-H2107
NCI-H889
kDA
34
97
X Empty well
**IgG heavy chain, 50 kDA
*IgG light chain, 25 kDA
G
SCLC-N
Input
IP
C N X IgG X α-NEUROD1
WB:
α-KPNB1
α-NEUROD1
NCI-H524
NCI-H2171
kDA
97
41
X Empty well

Figure 2

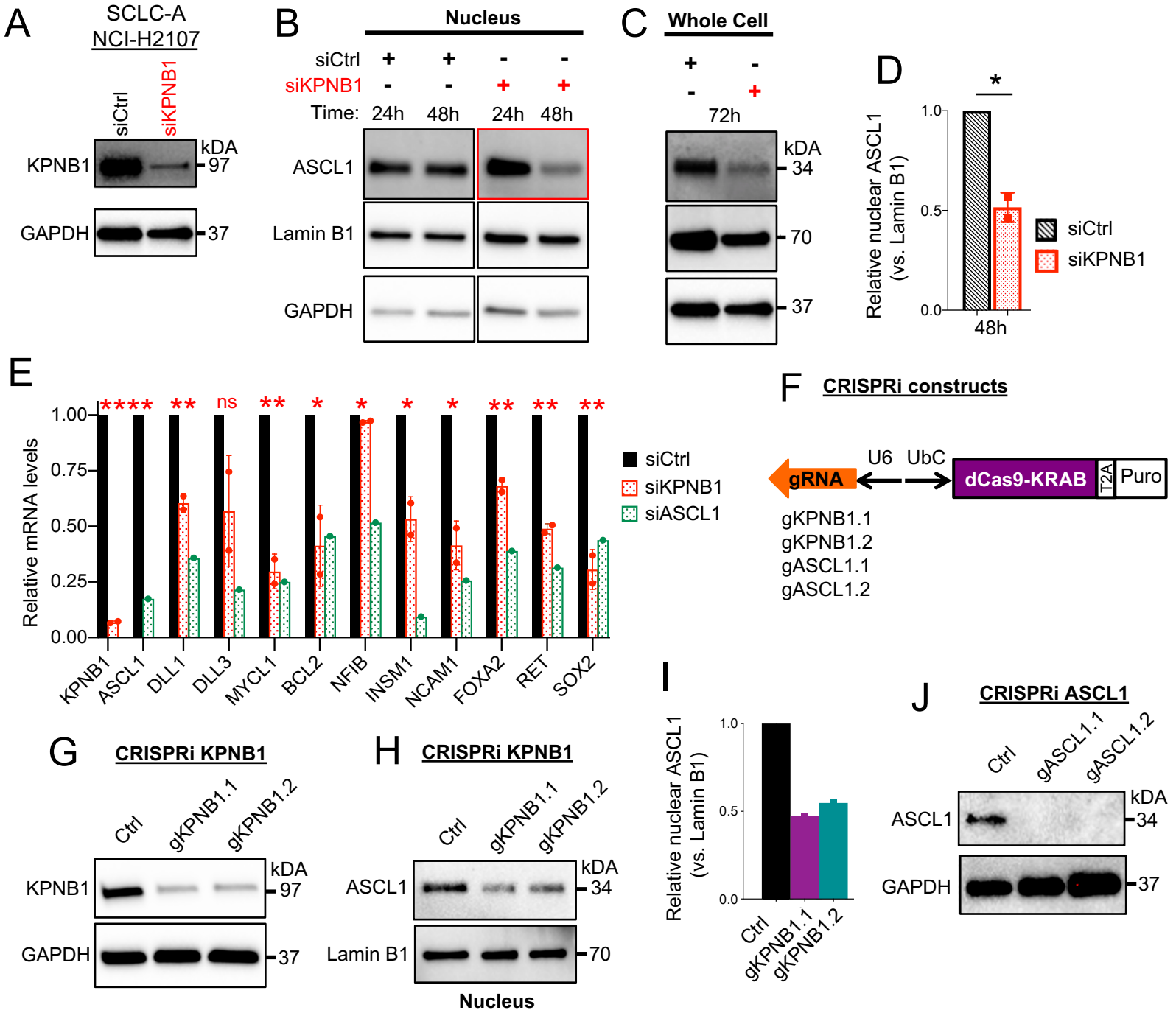
A
SCLC-A
NCI-H2107
siCtrl
siKPNB1
KPNB1
kDA
97
GAPDH
37
B
Nucleus
siCtrl + + - -
siKPNB1 - - + +
Time: 24h 48h 24h 48h
ASCL1
Lamin B1
GAPDH
C
Whole Cell
+ -
- +
72h
kDA
34
70
37
D
*
Relative nuclear ASCL1 (vs. Lamin B1)
1.0
0.5
0.0
48h
siCtrl
siKPNB1
E
**** ** ns ** * * * * ** ** **
Relative mRNA levels
1.00
0.75
0.50
0.25
0.00
KPNB1 ASCL1 DLL1 DLL3 MYCL1 BCL2 NFIB INSM1 NCAM1 FOXA2 RET SOX2
siCtrl
siKPNB1
siASCL1
F
CRISPRi constructs
gRNA
U6
UbC
dCas9-KRAB
T2A
Puro
gKPNB1.1
gKPNB1.2
gASCL1.1
gASCL1.2
G
CRISPRi KPNB1
Ctrl
gKPNB1.1
gKPNB1.2
KPNB1
kDA
97
GAPDH
37
H
CRISPRi KPNB1
Ctrl
gKPNB1.1
gKPNB1.2
ASCL1
kDA
34
Lamin B1
70
Nucleus
I
Relative nuclear ASCL1 (vs. Lamin B1)
1.0
0.5
0.0
Ctrl
gKPNB1.1
gKPNB1.2
J
CRISPRi ASCL1
Ctrl
gASCL1.1
gASCL1.2
ASCL1
kDA
34
GAPDH
37

Figure 2 Continued

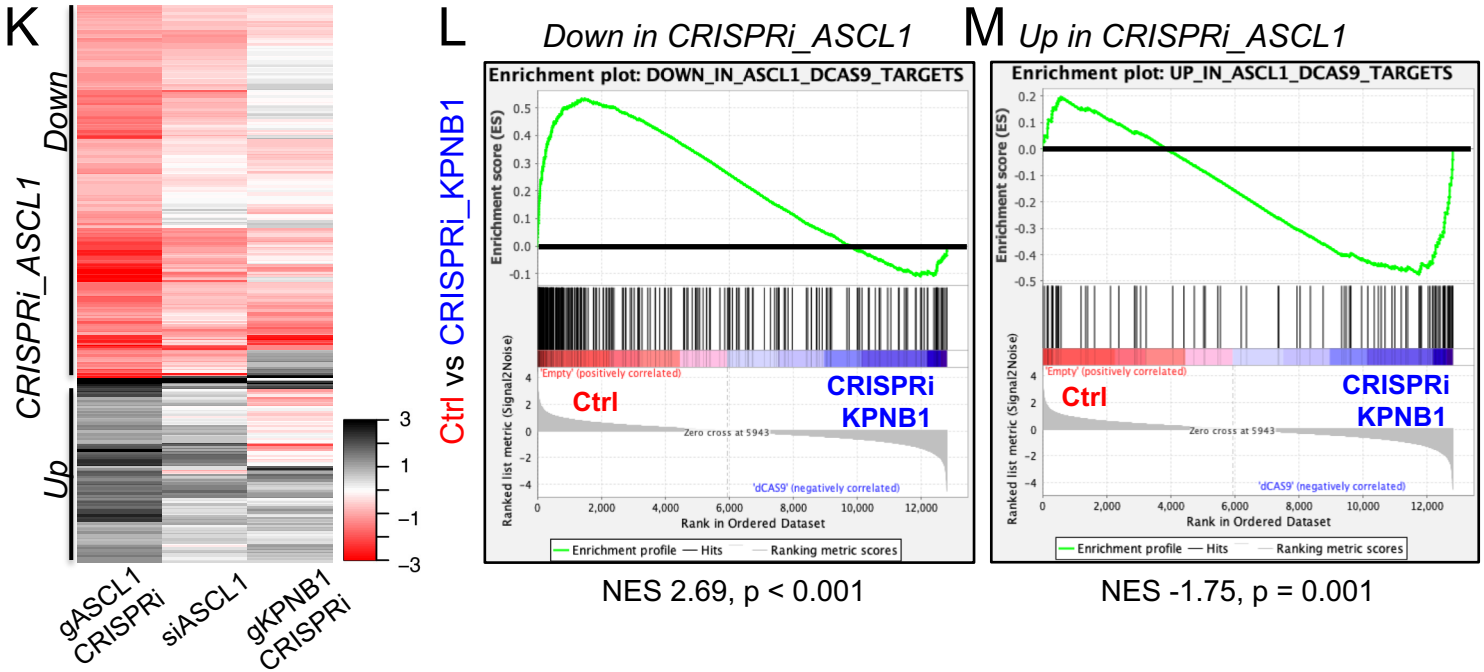

Figure 3

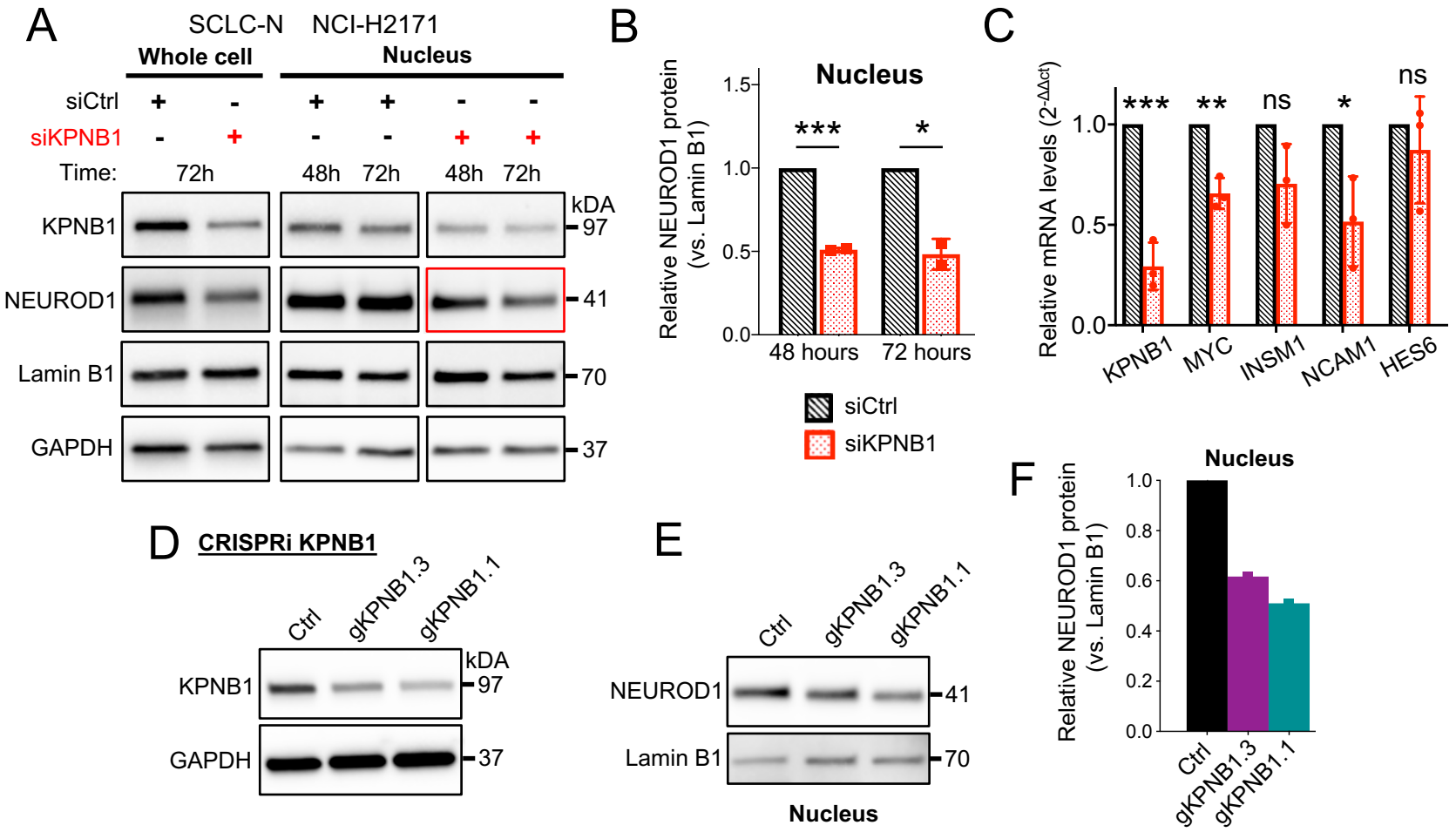
A
SCLC-N
NCI-H2171
Whole cell
Nucleus
siCtrl
siKPNB1
Time:
72h
48h
72h
48h
72h
KPNB1
NEUROD1
Lamin B1
GAPDH
kDA
97
41
70
37
B
Nucleus
Relative NEUROD1 protein (vs. Lamin B1)
1.5
1.0
0.5
0.0
***
*
48 hours
72 hours
siCtrl
siKPNB1
C
Relative mRNA levels (2-ΔΔct)
1.0
0.5
0.0
***
**
ns
*
ns
KPNB1
MYC
INSM1
NCAM1
HES6
D
CRISPRi KPNB1
Ctrl
gKPNB1.3
gKPNB1.1
KPNB1
GAPDH
kDA
97
37
E
Ctrl
gKPNB1.3
gKPNB1.1
NEUROD1
Lamin B1
41
70
Nucleus
F
Nucleus
Relative NEUROD1 protein (vs. Lamin B1)
1.0
0.8
0.6
0.4
0.2
0.0
Ctrl
gKPNB1.3
gKPNB1.1

Figure 4

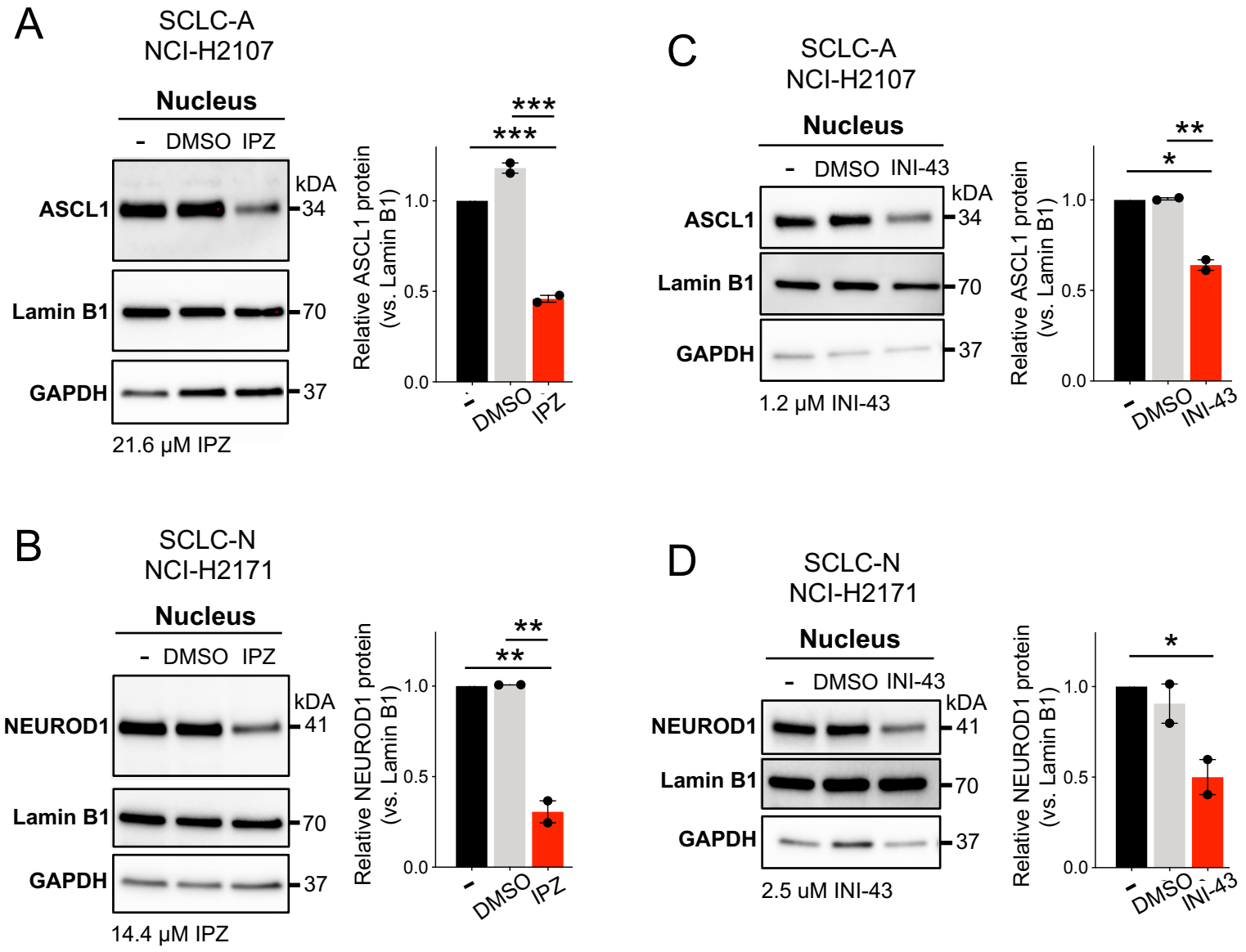
A
SCLC-A
NCI-H2107
Nucleus
- DMSO IPZ
kDA
ASCL1
34
Lamin B1
70
GAPDH
37
21.6 μM IPZ
Relative ASCL1 protein (vs. Lamin B1)
***
***
1.0
0.5
0.0
-
DMSO
IPZ
B
SCLC-N
NCI-H2171
Nucleus
- DMSO IPZ
kDA
NEUROD1
41
Lamin B1
70
GAPDH
37
14.4 μM IPZ
Relative NEUROD1 protein (vs. Lamin B1)
**
**
1.0
0.5
0.0
-
DMSO
IPZ
C
SCLC-A
NCI-H2107
Nucleus
- DMSO INI-43
kDA
ASCL1
34
Lamin B1
70
GAPDH
37
1.2 μM INI-43
Relative ASCL1 protein (vs. Lamin B1)
**
*
1.0
0.5
0.0
-
DMSO
INI-43
D
SCLC-N
NCI-H2171
Nucleus
- DMSO INI-43
kDA
NEUROD1
41
Lamin B1
70
GAPDH
37
2.5 uM INI-43
Relative NEUROD1 protein (vs. Lamin B1)
*
1.0
0.5
0.0
-
DMSO
INI-43

Figure 5

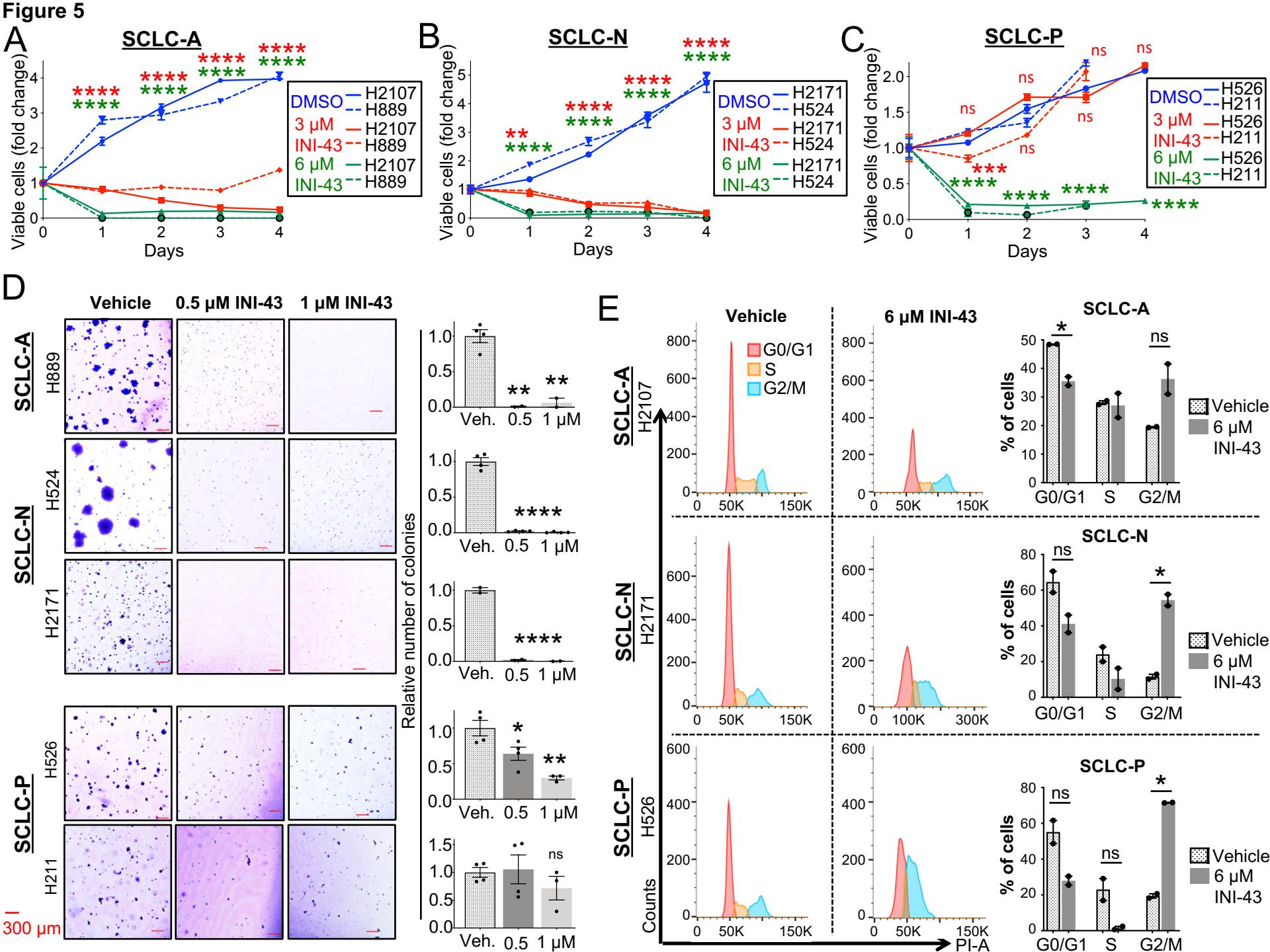
A
SCLC-A
Viable cells (fold change)
Days
DMSO H2107 H889
3 μM INI-43 H2107 H889
6 μM INI-43 H2107 H889
B
SCLC-N
Viable cells (fold change)
Days
DMSO H2171 H524
3 μM INI-43 H2171 H524
6 μM INI-43 H2171 H524
C
SCLC-P
Viable cells (fold change)
Days
DMSO H526 H211
3 μM INI-43 H526 H211
6 μM INI-43 H526 H211
D
Vehicle
0.5 μM INI-43
1 μM INI-43
SCLC-A
H889
SCLC-N
H524
H2171
SCLC-P
H526
H211
300 μm
Relative number of colonies
Veh. 0.5 1 μM
E
Vehicle
6 μM INI-43
SCLC-A
H2107
SCLC-N
H2171
SCLC-P
H526
G0/G1
S
G2/M
Counts
PI-A
% of cells
Vehicle
6 μM INI-43

Figure 6

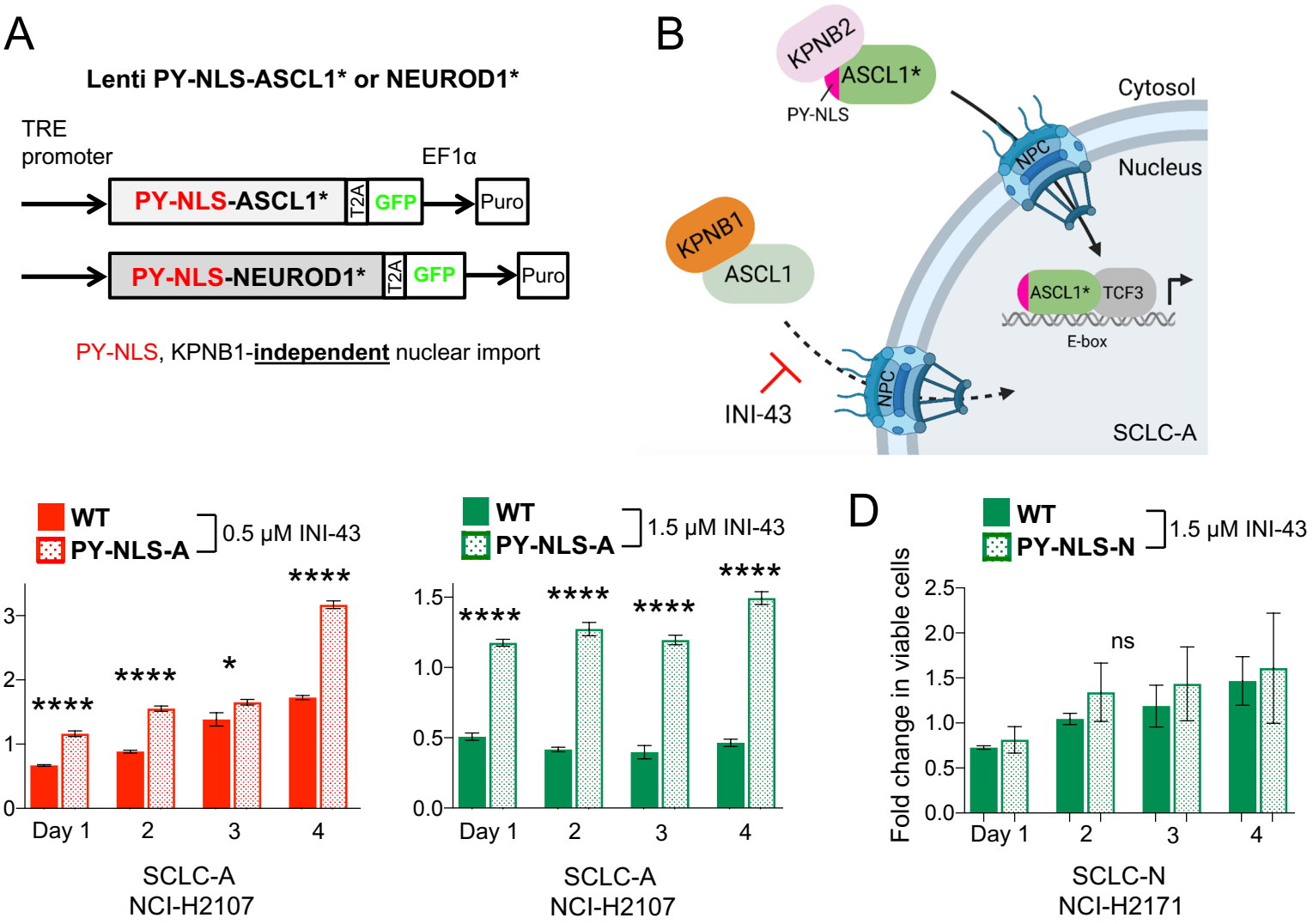
A
Lenti PY-NLS-ASCL1* or NEUROD1*
TRE promoter
EF1α
PY-NLS-ASCL1*
T2A
GFP
Puro
PY-NLS-NEUROD1*
T2A
GFP
Puro
PY-NLS, KPNB1-independent nuclear import
B
KPNB2
ASCL1*
PY-NLS
Cytosol
NPC
Nucleus
KPNB1
ASCL1
ASCL1*
TCF3
E-box
INI-43
NPC
SCLC-A
C
WT
PY-NLS-A
0.5 μM INI-43
Fold change in viable cells
****
****
*
****
Day 1
2
3
4
SCLC-A
NCI-H2107
WT
PY-NLS-A
1.5 μM INI-43
****
****
****
****
SCLC-A
NCI-H2107
D
WT
PY-NLS-N
1.5 μM INI-43
Fold change in viable cells
ns
Day 1
2
3
4
SCLC-N
NCI-H2171

Figure 7

A

	FPKM	
	LX44	LX22
KPNB1	113	115
ASCL1	860	17
NEUROD1	<1	140
POU2F3	<1	<1
YAP1	<1	<1